J. Fluid Mech. (1993), *vol.* 252, *pp.* 325–356

On the nonlinear dynamics of free bars in straight channels

By R. SCHIELEN[1, 2], A. DOELMAN[1] AND H. E. DE SWART[3]

[1] Mathematical Institute, Utrecht University, Budapestlaan 6, 3584 CP Utrecht, The Netherlands

[2] Delft Hydraulics, P.O. box 152, 8300 AD Emmeloord, The Netherlands

[3] Institute for Marine and Atmospheric Research Utrecht University, Princetonplein 5, 3584 CC, Utrecht, The Netherlands

(Received 13 March 1992 and in revised form 4 January 1993)

A simple morphological model is considered which describes the interaction between a unidirectional flow and an erodible bed in a straight channel. For sufficiently large values of the width–depth ratio of the channel the basic state, i.e. a uniform current over a flat bottom, is unstable. At near-critical conditions growing perturbations are confined to a narrow spectrum and the bed profile has an alternate bar structure propagating in the downstream direction. The timescale associated with the amplitude growth is large compared to the characteristic period of the bars. Based on these observations a weakly nonlinear analysis is presented which results in a Ginzburg–Landau equation. It describes the nonlinear evolution of the envelope amplitude of the group of marginally unstable alternate bars. Asymptotic results of its coefficients are presented as perturbation series in the small drag coefficient of the channel. In contrast to the Landau equation, described by Colombini *et al.* (1987), this amplitude equation also allows for spatial modulations due to the dispersive properties of the wave packet. It is demonstrated rigorously that the periodic bar pattern can become unstable through this effect, provided the bed is dune covered, and for realistic values of the other physical parameters. Otherwise, it is found that the periodic bar pattern found by Colombini *et al.* (1987) is stable. Assuming periodic behaviour of the envelope wave in a frame moving with the group velocity, simulations of the dynamics of the Ginzburg–Landau equation using spectral models are carried out, and it is shown that quasi-periodic behaviour of the bar pattern appears.

1. Introduction

The bed of most natural rivers consists of material which may be transported by currents. The interactions between river flow and the erodible boundaries result in the formation of morphological features such as bars, bends and meanders. Observations indicate that bars often occur as a series of propagating waves in the downstream direction with an alternating transversal amplitude structure. Typical wavelengths are of the order of the river width, the waves travel several metres each day and their amplitudes are approximately 80% of the undisturbed water depth. On the other hand river meanders have much larger characteristic scales than the bars. A better understanding of the behaviour of these phenomena is of interest, both from a practical and theoretical point of view.

In general the dynamics of morphological systems is rather complicated due to the strong feedback between currents and the various bedforms. Therefore, it becomes

worthwhile to consider simplified models in which a particular phenomenon may be investigated in isolation. The motivation is that these problems are more easy to deal with, but also yield information on the fundamental physical mechanisms. In many of such studies, including the present one, it is assumed that only the bottom is erodible and the river is modelled as an infinitely long straight channel. This eliminates the process of free river meandering, which is believed to be a secondary response on the formation of bars on the bottom or which may be generated by forcing mechanisms (Blondeaux & Seminara 1985; Crosato 1989).

The early studies on the dynamics of river bars were based on a linear instability theory, see Callander (1969), Engelund & Skovgaard (1973), Parker (1976), Fredsøe (1978,) Olesen (1983). They investigated the behaviour of small perturbations on a basic state describing a uniform current over a flat bottom. The result was a selection of the most unstable wavelength, for which alternate bars start to develop, if the width-to-depth ratio becomes sufficiently large. These theories, however, describe the initial stage of the evolution of the bars. If the amplitude becomes finite the linear theory is no longer valid because nonlinear terms become important.

The nonlinear evolution of bars was investigated by Colombini, Seminara & Tubino (1987) and Fukuoka (1989). They applied a weakly nonlinear theory for perturbations which grow on a timescale which is large compared to the typical period of the waves. The result of their two-timescale analysis was a so-called Landau equation describing the time evolution of the wave amplitude. It was demonstrated that all non-transient solutions of this equation are periodic and represent a finite-amplitude periodic alternate bar pattern. They only considered the case where the wavenumber is fixed in the neighbourhood of the critical wavenumber for which instability first occurs. This choice is disputable since in fact all waves in a narrow spectrum, centred around the critical wavenumber, are unstable. Owing to the dispersion of this wave group, modulations will also occur on a spatial scale. If this effect is included in the weakly nonlinear theory, a modified amplitude equation is found which is called the Ginzburg–Landau equation. Since the group velocity varies with the wavenumber we may expect this equation to describe local convergence and divergence of the perturbation energy, which may cause the periodic solutions obtained from the Landau theory to become unstable (Lighthill 1978). As a result bar patterns with a more complex temporal and spatial behaviour may be expected. Furthermore, it is possible to determine the stability of its solutions against general perturbations (in contrast to the Landau theory, where one can only study the stability of periodic solutions against perturbations with exactly the same wavenumber). The Ginzburg–Landau theory is therefore an essential extension of the Landau theory, and the aim of the present paper is to investigate the possible modified behaviour of bar patterns as described by the Ginzburg–Landau equation.

The Ginzburg–Landau equation has been derived for many physical systems such as Rayleigh–Bénard convection (Newell & Whitehead 1969), Poiseuille flow (Stewartson & Stuart 1971), or more recently, wind-driven water waves (Blennerhasset 1980), chemical processes (Kuramota 1984), binary fluid convection (Schöpf & Zimmerman 1989) etc. For morphological systems it has, to our knowledge, not yet been derived. Therefore in this paper a derivation of the Ginzburg–Landau equation will be presented for a simple morphological model and the behaviour of its solutions will be studied. The basic model, introduced in §2, describes the interaction between currents, forced by the inclination of a straight channel with fixed banks, and an erodible bottom. The sediment is assumed to be uniform and non-cohesive and is transported as bedload. The model has a basic state corresponding to a uniform flow over a flat

bottom. From the linear stability analysis of §3, a minimum width-to-depth ratio of the channel is obtained at which the basic state becomes unstable. This yields a critical wavenumber of the bed form perturbation which first starts to grow. For slightly larger values of the width-to-depth ratio a weakly nonlinear theory will be applied in §4 which results in the Ginzburg–Landau equation. This equation describes the nonlinear dynamics of the envelope amplitude of a packet of marginally unstable free bars, and the coefficients are presented in terms of the original morphological parameters, which are the friction coefficient, width-to-depth ratio and the sediment transport coefficients. In §5 solutions of the Ginzburg–Landau equation and the corresponding bed profiles are discussed. The analysis of the mathematical properties of the Ginzburg–Landau equation has been the subject of many papers. Results of Keefe (1985), Doering *et al.* (1988) and Doelman (1989, 1991) demonstrate the possibility of periodic, quasi-periodic and chaotic solutions. However, for the present morphological model a less rich behaviour is found for realistic choices of the parameters. It will be demonstrated that the periodic alternate bar pattern, obtained by Colombini *et al.* (1987) using Landau theory, can be unstable when the bed is dune covered. The subsequent dynamical behaviour is investigated by using a spectral model of the Ginzburg–Landau equation. The results show that quasi-periodic bar patterns are found instead. A discussion of these results and some conclusions are presented in the final section.

We would like to emphasize that the main purpose of this paper is the derivation and the analysis of the modulation equation. To simplify our presentation we have considered a model for the process of river bed evolution which only has the most essential features necessary to describe the main characteristics of this process. Therefore, we did not consider important effects in our model such as the variation of the drag coefficient (Einstein 1950; Colombini *et al.* 1987), the variation of the bed slope coefficient (Sekine & Parker 1992), the effect of secondary currents (Rozovskij 1957) etc. This probably means that the predictions based on our analysis will only give crude indications of what happens in nature. However, comparisons with earlier studies on the linear and nonlinear analysis have been made and our results were found to be in good agreement with these studies. Furthermore, our model problem can be extended to a more realistic model which can be studied by exactly the same techniques. We based our analysis on the simple model to minimize the amount of mathematical computations and to facilitate the presentation. The (weakly) nonlinear pattern formation in a realistic model will also be governed by the same modulation equation (only the coefficients will be in a different range). This modulation equation is the most general tool in nonlinear stability theory: by its mathematical nature it governs all possible pattern generating processes (Newell 1974). We therefore emphasize in this paper the structure which is present in morphological processes, a structure which enables us to analyse and predict patterns of a non-periodic (or even chaotic) kind.

2. The model

We consider a depth-averaged shallow water flow in a straight, infinitely long channel, having a uniform (mild) slope, which we denote by $i_0 \ll 1$. Further, we consider the banks to be non-erodible, whereas the bottom consists of non-cohesive sediment, which we assume to be transported as bedload. A situation sketch is presented in figure 1. It is clear that for using a depth-averaged model the channel width should be much larger than the undisturbed water depth. This also motivates the neglect of horizontal diffusion of momentum, since this effect is confined to thin

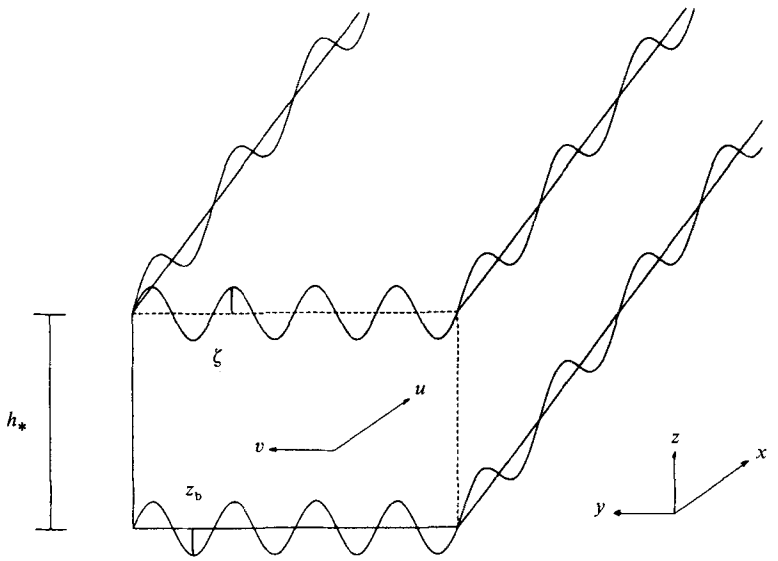

FIGURE 1. Sketch of the physical situation studied.

boundary layers along the sidewalls which are not of interest for the present analysis. Furthermore, it can be demonstrated *a posteriori* that the effect of flow separation, caused by the resulting bedforms, may be ignored. This implies that the bar amplitudes should be much smaller than their characteristic horizontal scales. This appears to be the case for the present features, as was already found by Colombini *et al.* (1987).

The equations of motion then become

$$\frac{\partial \boldsymbol{U}}{\partial t} + (\boldsymbol{U}\cdot\boldsymbol{\nabla})\,\boldsymbol{U} + g\boldsymbol{\nabla}\zeta = \mathscr{F}, \tag{2.1}$$

$$\frac{\partial(\zeta - z_b)}{\partial t} + \boldsymbol{\nabla}\cdot(\boldsymbol{U}(\zeta + h_* - z_b)) = 0, \tag{2.2}$$

$$\frac{\partial z_b}{\partial t} + \boldsymbol{\nabla}\cdot\boldsymbol{S} = 0. \tag{2.3}$$

As shown in figure 1, we use an orthogonal coordinate system, where we assume that the α-direction coincides with the streamwise direction. In (2.1)–(2.3) $\boldsymbol{U} = (u, v)$ is the depth-averaged velocity in the x- and y-directions, ζ is the elevation of the disturbed free surface with respect to the undisturbed water depth h_*, and z_b is the disturbed bed level with respect to the undisturbed water depth. The nabla-operator is defined as $\boldsymbol{\nabla} = (\partial/\partial x, \partial/\partial y)$.

The vector $\mathscr{F}$ represents the forcing and friction mechanisms, which we model as

$$\mathscr{F} = \left(-C\frac{u(u^2+v^2)^{\frac{1}{2}}}{\zeta - z_b + h_*} + i_0 g, -C\frac{v(u^2+v^2)^{\frac{1}{2}}}{\zeta - z_b + h_*} \right). \tag{2.4}$$

Note that this means that we model the bottom stress in the direction of the depth-averaged velocity.

In (2.1)–(2.4), $C = g/C_f^2$, the drag coefficient, where g is acceleration due to gravity and C_f is the Chézy coefficient. We assume that the bottom evolution only depends on

the local flow parameters. The volumetric sediment flux $\boldsymbol{S}$, with components S_x and S_y in the x- and y-directions respectively, is modelled as

$$\boldsymbol{S} = \sigma |\boldsymbol{U}|^b \left(\frac{\boldsymbol{U}}{|\boldsymbol{U}|} - \gamma \nabla z_b \right) \tag{2.5}$$

for some $b > 0$ and $\gamma > 0$; σ depends on the bed porosity and on the sediment properties. Note that $b > 3$ corresponds to a dune-covered bed. Many transport formulae are of this type, see the review in van Rijn (1989). Note that we omit the effect of secondary flow on the direction of the sediment transport. It is noted by Parker & Johannesson (1989) that in the case of a straight channel this is a secondary effect which may be neglected. Since our aim is to consider a simple conceptual model, which only contains the essential physical mechanisms responsible for morphological instabilities, we take constant values for the parameters b, C and γ. In fact, accurate values for b are unknown and typical choices range between 2 and 7, see the review by van Rijn (1989). A physically more realistic choice for the drag coefficient would be the parameterization suggested by Einstein (1950); however, we consider the variation on the local water depth to be a higher-order effect. Finally, a constant γ corresponds to the simple expressions derived by Bagnold (1956) and Engelund (1974), in which it represents the inverse of the dynamic coefficient of Coulomb friction. More general expressions for γ, including dependence on the bottom stress, are discussed by Sekine & Parker (1992). We have taken γ of order 1 throughout our analysis.

We close the model by the following boundary conditions:

$$v = 0, \quad S_y = 0 \quad \text{on} \quad \Gamma, \tag{2.6}$$

where we denote by Γ the walls, i.e. $y = 0$ and $y = y_*$. These boundary conditions represent the assumption that the walls are impermeable for water as well as sediment. From (2.5) and (2.6) it easily follows that $\partial z_b / \partial y = 0$ on Γ.

Note that the model allows for a steady uniform flow in the downslope direction, the magnitude of which is determined by a balance between forcing and dissipation (see (2.4)). If we denote the corresponding variables with an asterisk, it follows that

$$u_*^2 = i_0 g h_* / C, \quad v_* = 0, \quad \zeta_* = 0, \quad z_{b*} = 0. \tag{2.7}$$

The next step in the analysis is to make the variables dimensionless. This is done in the following way: we substitute

$$\left.\begin{aligned} &\boldsymbol{U} = (u, v) = u_* \hat{\boldsymbol{U}}; \quad z_b = h_* \hat{z}_b; \quad \boldsymbol{X} = (x, y) = y_* (\hat{\boldsymbol{X}}), \\ &\zeta = \frac{u_*^2}{g} \hat{\zeta}; \quad t = \frac{y_* h_*}{\sigma u_*^b} \hat{t} = T \hat{t}. \end{aligned}\right\} \tag{2.8}$$

The scaling for ζ is motivated by the fact that the pressure force tends to zero if u_* tends to zero, independent of the value for C. Thus there must be a balance between the advection terms and the pressure gradient. The scaling for the time means that we scale with the morphological timescale. This should be clear since we are interested in bedform instabilities which occur on this timescale.

Substitution of (2.7) in (2.1)–(2.3) yields the following model for the scaled quantities (hats are dropped for convenience):

$$\kappa \frac{\partial u}{\partial t} + u \frac{\partial u}{\partial x} + v \frac{\partial u}{\partial y} + \frac{\partial \zeta}{\partial x} = -CR \left(-1 + \frac{u(u^2 + v^2)^{\frac{1}{2}}}{F^2 \zeta + 1 - z_b} \right), \tag{2.9}$$

$$\kappa\frac{\partial v}{\partial t}+u\frac{\partial v}{\partial x}+v\frac{\partial v}{\partial y}+\frac{\partial \zeta}{\partial y}=-CR\left(\frac{v(u^2+v^2)^{\frac{1}{2}}}{F^2\zeta+1-z_b}\right), \tag{2.10}$$

$$\kappa F^2\frac{\partial \zeta}{\partial t}-\kappa\frac{\partial z_b}{\partial t}+\frac{\partial}{\partial x}\{u(F^2\zeta+1-z_b)\}+\frac{\partial}{\partial y}\{v(F^2\zeta+1-z_b)\}=0, \tag{2.11}$$

$$\frac{\partial z_b}{\partial t}+\frac{\partial S_x}{\partial x}+\frac{\partial S_y}{\partial y}=0. \tag{2.12}$$

Here
$$\boldsymbol{S}=(S_x,S_y)=|\boldsymbol{U}|^b\left(\frac{\boldsymbol{U}}{|\boldsymbol{U}|}-\frac{\gamma}{R}\nabla z_b\right) \tag{2.13}$$

and
$$R=y_*/h_*,\quad F=u_*/(gh_*)^{\frac{1}{2}},\quad \kappa=y_*/u_*\,T, \tag{2.14}$$

which are the width-to-depth ratio of the channel, the Froude number and the ratio of the timescale of flow adaption and the morphological timescale, respectively.

We shall now simplify the model (2.9)–(2.12) by applying two approximations. First it is observed that the flow responds to a change in the bottom by generating travelling gravity waves. This adjustment process is controlled by dissipation, the characteristic timescale of which is assumed to be larger than (or of the same order as) the advective timescale y_*/u_*, but small compared to the morphological timescale T. This implies that κ in (2.9)–(2.12) is very small. We may therefore omit the time derivatives in the flow equations, which means that the flow instantaneously adapts to the evolution of the bed (quasi-stationary approach).

The second approximation is related to the observation that many river flows have a small Froude number. Thus we shall neglect in (2.9)–(2.12) all terms containing the parameter F, which means that we apply the rigid-lid approximation. An additional motivation for this step follows from the results of the linear theory to be discussed in the next section. It appears that in the limit $F\to 0$ the calculations simplify considerably whereas essential physical mechanisms determining bed form instabilities are still included. On the other hand it implies that the possible applicability of our model to laboratory experiments, where Froude numbers are often of order 1 or larger, is limited.

The above considerations lead to the following model, which we shall use as starting point for the subsequent analysis:

$$u\frac{\partial u}{\partial x}+v\frac{\partial u}{\partial y}+\frac{\partial \zeta}{\partial x}=-CR\left(-1+\frac{u(u^2+v^2)^{\frac{1}{2}}}{1-z_b}\right), \tag{2.15}$$

$$u\frac{\partial v}{\partial x}+v\frac{\partial v}{\partial y}+\frac{\partial \zeta}{\partial y}=-CR\left(\frac{v(u^2+v^2)^{\frac{1}{2}}}{1-z_b}\right), \tag{2.16}$$

$$\frac{\partial}{\partial x}\{u(1-z_b)\}+\frac{\partial}{\partial y}\{v(1-z_b)\}=0, \tag{2.17}$$

$$\frac{\partial z_b}{\partial t}+\frac{\partial S_x}{\partial x}+\frac{\partial S_y}{\partial y}=0, \tag{2.18}$$

with R, S_x and S_y as in (2.13)–(2.14).

It is readily observed that a basic state of the scaled model is given by

$$(u_0,v_0,\zeta_0,z_{b_0})=(1,0,0,0). \tag{2.19}$$

3. Linear theory

In this section we study the linear stability of the basic state $\phi_0 = (u_0, v_0, \zeta_0, z_{b_0})$ defined in (2.19). Although this kind of analysis is quite standard we shall present results in some detail, since the nonlinear theory, developed in §4, is based on the linear analysis. We study the stability of the basic state by considering the evolution of small perturbations. Thus we substitute in (2.15)–(2.18)

$$\boldsymbol{\phi} \equiv (u, v, \zeta, z_b) = \boldsymbol{\phi}_0 + \boldsymbol{\phi}' \tag{3.1}$$

and neglect nonlinear terms to find four linear partial differential equations. They may be symbolically written as

$$\boldsymbol{L}\boldsymbol{\phi}' = 0, \tag{3.2}$$

where the elements of the 4×4 matrix $\boldsymbol{L}$ contain known partial derivatives with respect to x, y and t:

$$\boldsymbol{L} = \begin{pmatrix} \dfrac{\partial}{\partial x} + 2CR & 0 & \dfrac{\partial}{\partial x} & CR \\ 0 & \dfrac{\partial}{\partial x} + CR & \dfrac{\partial}{\partial y} & 0 \\ \dfrac{\partial}{\partial x} & \dfrac{\partial}{\partial y} & 0 & -\dfrac{\partial}{\partial x} \\ b\dfrac{\partial}{\partial x} & \dfrac{\partial}{\partial y} & 0 & \dfrac{\partial}{\partial t} - \dfrac{\gamma}{R}\left(\dfrac{\partial^2}{\partial x^2} + \dfrac{\partial^2}{\partial y^2}\right) \end{pmatrix}. \tag{3.3}$$

The channel geometry allows for travelling wave solutions in the x-direction with unknown lateral structure. Thus we substitute in (3.2)

$$\boldsymbol{\phi}' = \boldsymbol{f}(y)\, \mathrm{e}^{\mathrm{i}kx + \omega t} + \text{c.c.} \quad \text{with} \quad \boldsymbol{f}(y) = (\hat{u}(y), \hat{v}(y), \hat{\zeta}(y), \hat{z}_b(y)), \tag{3.4}$$

where k is a real-valued wavenumber, ω the complex frequency, c.c. denotes complex conjugate and $\boldsymbol{f}(y)$ represents the amplitudes. We reduce the four equations to one equation for $\hat{z}_b$ by Gauss elimination, resulting in a fourth-order differential equation

$$L\hat{z}_b(y) \equiv b_3 \frac{\mathrm{d}^4 \hat{z}_b}{\mathrm{d}y^4} + (\omega a_2 + b_2)\frac{\mathrm{d}^2 \hat{z}_b}{\mathrm{d}y^2} + (\omega a_1 + b_1)\hat{z}_b(y) = 0, \tag{3.5}$$

with boundary conditions $\mathrm{d}\hat{z}_b/\mathrm{d}y = \mathrm{d}^3\hat{z}_b/\mathrm{d}y^3 = 0$ on Γ (i.e. for $y = 0$, $y = 1$).

In (3.5)

$$\begin{aligned} b_3 &= -(\gamma/R)(\mathrm{i}k + 2CR), \\ b_2 &= 2\mathrm{i}k^3(\gamma/R) + k^2(-1 + 3C\gamma) + \mathrm{i}kCR(3 - b), \\ b_1 &= -\mathrm{i}k^5(\gamma/R) + k^4(-C\gamma + b) - \mathrm{i}k^3 CRb, \\ a_2 &= 2RC + \mathrm{i}k, \quad a_1 = -\mathrm{i}k^3 - k^2 CR. \end{aligned}$$

Equation (3.5) is an eigenvalue problem which admits solutions of the form $\hat{z}_b(y) = \mathrm{e}^{\mu y}$. Substitution of this expression in (3.5) gives

$$\mu^4 b_3 + \mu^2(\omega a_2 + b_2) + (\omega a_1 + b_1) = 0, \tag{3.6}$$

an equation which is quadratic in μ, with roots μ_1^2, μ_2^2. The solution of (3.5) then reads:

$$\hat{z}_b(y) = A_1 \mathrm{e}^{\mu_1 y} + A_2 \mathrm{e}^{-\mu_1 y} + A_3 \mathrm{e}^{\mu_2 y} + A_4 \mathrm{e}^{-\mu_2 y}$$

and applying the boundary conditions yields the eigenfunctions

$$\hat{z}_b(y) = A\cos(p\pi y), \quad p = 1, 2, \ldots, \tag{3.7}$$

where A is an arbitrary amplitude. Thus in (3.5) the eigenvalues should have the value

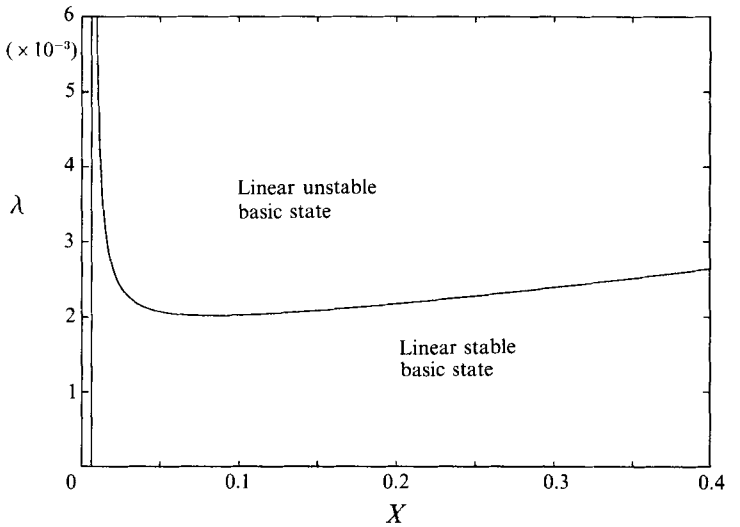

FIGURE 2. Neutral curve for the parameter values $b = 5$, $C = 0.007$ and $\gamma = 1$, thus $\delta = 0.0017$ (δ is defined in (3.11)).

$p\pi i$. Then by back substitution into the four algebraic equations relating the amplitudes of the perturbation we recover for the vector $\boldsymbol{f}(y)$ the following:

$$\boldsymbol{f}(y) = A \begin{pmatrix} \alpha_u \cos(p\pi y) \\ \alpha_v \sin(p\pi y) \\ \alpha_\zeta \cos(p\pi y) \\ \cos(p\pi y) \end{pmatrix} \equiv A\boldsymbol{\Phi}$$

with

$$\alpha_u = \frac{-(k^2\gamma/R + ik + \omega + \pi^2\gamma/R)}{(b-1)ik}, \quad \alpha_v = -\frac{ik(\alpha_u - 1)}{\pi p}, \quad \alpha_\zeta = \frac{(ik + CR)\alpha_v}{\pi p}. \tag{3.8}$$

Hence, the lateral structure of the wave solution is now known and can be denoted with $\boldsymbol{\phi}' = A\boldsymbol{\Phi}E$ where $E = e^{ikx+\omega t}$.

Finally, the frequency ω is related to the wavenumber k by a dispersion relation, as follows from (3.6):

$$\omega = \frac{p^4\pi^4 b_3 - p^2\pi^2 b_2 + b_1}{p^2\pi^2 a_2 - a_1}. \tag{3.9}$$

It is obvious from (3.4) that the stability of the basic state is determined by the real part of ω. If the real part ω_r of ω is smaller than 0, perturbations of the kind (3.4) decay exponentially in time, i.e. the basic state is stable. Accordingly, if ω_r is greater than zero, we are dealing with exponentially growing solutions, i.e. an unstable basic state. Hence, $\omega_r = 0$, the so-called neutral curve, is a separatrix between the exponentially growing and decaying solutions of the linear problem. Using (3.9) we derive a formula describing the neutral curve:

$$\lambda = \frac{-X(X+1)^3\delta}{\delta(X+1)(X+2)^2 - X(2X+1)}, \tag{3.10}$$

with

$$\lambda = \frac{C^2R^2}{p^2\pi^2}, \quad X = \frac{k^2}{p^2\pi^2}, \quad \delta = \frac{\gamma C}{\beta}, \quad \beta = b-1. \tag{3.11}$$

In figure 2 we have plotted the neutral curve for a fixed value of δ which lies in the physically interesting area. We observe that for a width-to-depth ratio R smaller than

a certain critical value R_c, all perturbations decay exponentially. For $R > R_c$ a range of linear waves have positive growth rate ($\omega_r > 0$) and consequently the basic state is unstable. We expect interesting behaviour of the perturbations if R passes through R_c, i.e. when the basic state looses its stability properties. It turns out that varying R is a good starting point for studying the dynamics of our underlying system.

Let us finally make a more detailed observation about the position of the minima of the neutral curves as a function of p. If we denote by $(k_c(p), R_c(p))$ the minimum as function of p, it is clear from (3.10) that

$$(k_c(p), R_c(p)) = p(k_c(1), R_c(1)).$$

This means that increasing p leads to a higher minimum of the neutral curve and a larger critical wavenumber. Thus, the ($p = 1$)-mode (the situation of alternate bars) is the first mode that becomes unstable. Therefore, we may restrict our attention on the case $p = 1$.

From now on a subscript 'c' means the evaluation of operators and functions at critical conditions, i.e. at $k = k_c$, $R = R_c$. So for instance, $\boldsymbol{\Phi}_c = \boldsymbol{\Phi}|_{\substack{k=k_c \\ R=R_c}}$. The linear solution of the problem at critical conditions then reads

$$\boldsymbol{\phi}_l = \boldsymbol{\phi}'_c = A\boldsymbol{\Phi}_c E_c, \tag{3.12}$$

where $\boldsymbol{\Phi}$ follows from (3.8) and $E_c = e^{ik_c x + \omega_c t}$. In order to obtain a better understanding of the neutral curve we perform a perturbation analysis with respect to the small parameter $\delta = \gamma C/\beta$. For realistic choices of the morphological parameters, typical values for δ range between 0.0001 and 0.01. Although this expansion is in principle unnecessary, it provides predictions concerning the bar formation which depend explicitly (instead of implicitly) on the model parameters b, C and γ. Therefore, this approach yields a better insight in the fundamental behaviour of the model. Then, using (3.10) two physically interesting roots of the denominator appear:

$$x_1 = 4\delta + O(\delta^2), \tag{3.13}$$

$$x_2 = 2/\delta - \tfrac{9}{8} + O(\delta), \tag{3.14}$$

i.e. there are no destabilizing waves with wavenumbers outside the interval described by these two asymptotes. The asymptotic expressions for k_c and R_c read

$$k_c = \sqrt{2}\,\pi\delta^{\frac{1}{4}}\{1 + \tfrac{19}{4}\delta + O(\delta^{\frac{3}{2}})\}, \tag{3.15}$$

$$R_c = (\pi\gamma/\beta)\,\delta^{-\frac{1}{2}}\{1 + 2\delta^{\frac{1}{2}} + 4\delta + O(\delta^{\frac{3}{2}})\}, \tag{3.16}$$

and we derive the asymptotic expression for ω_c from (3.9)

$$\omega_c = -ik_c\{1 + \beta\delta^{\frac{1}{2}} - 5\beta\delta + O(\delta^{\frac{3}{2}})\}. \tag{3.17}$$

Note that $|i\omega_c|$ is the wave frequency at critical conditions. Asymptotic expressions for α_u, α_v, α_ζ are given in Appendix A.

The physical mechanism of instability can be understood from a closer investigation of the perturbation equations (3.1)–(3.2). In order to obtain unstable bedform disturbances the morphological system should allow for convergence of sediment at the wave crests. As described by the evolution equation for the bottom this requires a phase difference between the divergence of the sediment transport and the bottom disturbances that is between $\frac{1}{2}\pi$ and $\frac{3}{2}\pi$. Here only the transport corresponding to $\gamma = 0$ needs to be considered, since the downslope term in the total transport always causes damping of the perturbations. It follows straightforwardly from (3.2)–(3.3) that in the cases $CR = 0$ (no bottom friction), $b = 1$ or $v' = 0$ (a one-dimensional model)

this phase difference is exactly $\frac{1}{2}\pi$ or $\frac{3}{2}\pi$. This implies that perturbations will decay by diffusive mechanisms, due to the downslope correction term in the volumetric sediment transport. Some of these results follow directly from combination of the two linearized continuity equations in (3.2)–(3.3), yielding

$$\frac{\partial z_b'}{\partial t} + b\frac{\partial z_b'}{\partial x} - \frac{\gamma}{R}\nabla^2 z_b' = \beta\frac{\partial v'}{\partial y}. \tag{3.18}$$

This is an advection–diffusion equation which, in the absence of forcing on the right-hand side, describes decaying travelling wave solutions. Obviously, necessary conditions for the occurrence of unstable free bars are a two-dimensional model and the presence of bottom friction. On the other hand the latter mechanism also causes direct damping of the perturbations. This implies that the energy flux from the basic flow to the perturbations should exceed the dissipation of energy due to bottom friction. The energy gain is provided for by advection terms in the equations of motion, which in the linear theory are proportional to the wavenumber k. Thus instabilities cannot occur in the limit $k \to 0$, i.e. long waves are stable. On the other hand, the diffusive terms in the sediment continuity equation are proportional to $\gamma k^2/R$ and thus cause stabilization of the short waves. The combined effect of bottom friction and the downslope correction term in the volumetric sediment transport results in a critical width-to-depth ratio below which all waves are stable. The long- and short-wave cut-offs are described by the asymptotic results (3.13) and (3.14). In figure 2 only the long-wave asymptote of the neutral curve is visible. We remark that the stabilization of short waves in the model of Colombini *et al.* (1987) cannot be explained in this sense, since they neglect longitudinal bed slope corrections in the parameterization of the sediment transport. On the other hand, they allow for a drag coefficient depending on the local bed roughness as well as for free surface effects, which are important when the Froude number is not small. Both mechanisms appear to cause an effective damping of perturbations with large wavenumbers.

For realistic values of the morphological parameters we find critical width-to-depth ratios between 20 and 30, critical wavelengths between 5 and 15 channel widths and wave periods between 5 and 15 morphological timescale units. We have compared these predictions with those of previous linear stability studies concerning free bars in straight channels. In particular the results of Engelund & Skovgaard (1973), Fredsoe (1978) and Colombini *et al.* (1987) are relevant because their models include the important effect of bed slope correction terms in the sediment transport. In all of these studies it is demonstrated that the agreement of the theoretical findings with observations is quite satisfactory. At this point we recall that our model contains three major simplifications compared to the other models, i.e. free surface effects, the variation of the drag coefficient with the local water depth and the presence of a critical shear stress for erosion are neglected. Despite these rather rigorous simplifications the results of our linear stability analysis are in good agreement with those of the previous studies. In particular it follows from Colombini *et al.* (1987) that in the low Froude number regime their critical width-to-depth ratios $\beta_c \equiv \frac{1}{2}R_c$ ranges between 10 and 15, whereas their critical wavelengths are 6 to 12 river width units.

4. Weakly nonlinear theory

In the previous section it has been demonstrated that for width-to-depth ratios larger than a critical value R_c the basic state of our model, i.e. a uniform flow over a flat bed, is unstable. The linear theory shows that in this case a spectrum of wave-like

perturbations with exponentially growing amplitudes will develop. However, this description is only valid in the initial growth stage, where the wave amplitudes are infinitesimally small. If we want to describe the nonlinear dynamic behaviour, we must take into account the nonlinear interactions between the various (linearly unstable) wave components. A detailed analysis is possible if the width-to-depth ratio R is only slightly larger than the critical value R_c. Therefore, we restrict ourselves to width-to-depth ratios R, for which

$$R = R_c(1+\hat{r}\epsilon^2) = R_c + r\epsilon^2 \quad \text{where} \quad \epsilon \ll 1, \quad \hat{r} = O(1), \quad r = O(R_c). \tag{4.1}$$

From a mathematical point of view, parameter ϵ should be 'small enough' in order to be able to perform a perturbation analysis. The nonlinear theory described below has been applied to various classical hydrodynamic stability problems (see for instance Newell & Whitehead 1969; Stewartson & Stuart 1971) and has been tested experimentally (see for instance Drazin & Reid 1981 for an overview). In these experiments it has been found that the predictions based on the (weakly) nonlinear theory might be valid for R/R_c considerably larger than 1, i.e. physically, the theory seems to be valid for ϵ of an order-1 magnitude.

Because the neutral curve can be approximated by a parabola near its minimum, we consider wavenumbers k for which

$$|k-k_c| = O(\epsilon), \quad \epsilon \ll 1. \tag{4.2}$$

The unstable waves are thus limited to a narrow spectrum around the critical wavenumber k_c. Besides, the waves are marginally unstable: they grow on a timescale which is large compared to the typical wave periods. The consequence of these assumptions can be seen by expanding the complex frequency ω in a Taylor series near (k_c, R_c):

$$\omega = \tau_r(R-R_c) + \tfrac{1}{2}\tau_{k^2}(k-k_c)^2 + \ldots + \omega_c + \mathrm{i}[\nu_k(k-k_c) + \nu_r(R-R_c) + \tfrac{1}{2}\nu_{k^2}(k-k_c)^2 + \ldots], \tag{4.3}$$

where

$$\tau_r + \mathrm{i}\nu_r = \left(\frac{\partial\omega}{\partial R}\right)_c, \quad \mathrm{i}\nu_k = \left(\frac{\partial\omega}{\partial k}\right)_c, \quad \tau_{k^2} + \mathrm{i}\nu_{k^2} = \left(\frac{\partial^2\omega}{\partial k^2}\right)_c, \tag{4.4}$$

where 'c' means, as before, evaluation at critical conditions. Here τ_r-measures the growth rate of the marginally unstable waves, whereas ν_r gives the frequency shift of the perturbation with respect to the basic wave. Furthermore, ν_k is the group velocity of the wave packet; τ_{k^2} and ν_{k^2} will be interpreted later on. Note that ω_c in (4.3) is an imaginary number, as defined in (3.17).

Substitution of (4.3) in the linear solution of the bottom perturbation (3.4) yields

$$\begin{aligned} z_b &\sim \mathrm{e}^{\mathrm{i}kx+\omega t} + \ldots + \text{c.c.}, \\ &= \mathrm{e}^{\mathrm{i}k_c x+\omega_c t}\,\mathrm{e}^{\mathrm{i}(k-k_c)(x+\nu_k t)} \exp[\{\tau_r(R-R_c) + \tfrac{1}{2}\tau_{k^2}(k-k_c)^2\}t] + \ldots + \text{c.c.}, \qquad (4.5) \\ &= A(\xi,\tau)\,E_c + \ldots + \text{c.c.} \qquad (4.6) \end{aligned}$$

This describes (the modulation of) a basic critical wave with wavenumber k_c and frequency ω_c. The modulation is at slow temporal and spatial scales, which are described by the coordinates

$$\tau = \epsilon^2 t, \quad \xi = \epsilon(x+\nu_k t), \tag{4.7}$$

where (4.1) and (4.2) are used. Note that we thus have introduced a long timescale τ and a long spatial scale ξ which is a slow, moving coordinate, travelling with the group

velocity. This is because the envelope of a linear dispersive wave packet travels with this velocity. This behaviour suggests the use of multiple scale analysis in order to obtain an evolution equation for the amplitude $A(\xi,\tau)$.

Note also that the proposed scaling has an influence in the set of equations (2.15)–(2.18):

$$\frac{\partial}{\partial t}\to\frac{\partial}{\partial t}+\epsilon^2\frac{\partial}{\partial\tau}+\epsilon\nu_k\frac{\partial}{\partial\xi},\quad \frac{\partial}{\partial x}\to\frac{\partial}{\partial x}+\epsilon\frac{\partial}{\partial\xi}. \tag{4.8}$$

Since we expect that solutions of the full system will be small for R close to R_c we expand

$$\boldsymbol{\phi}=\boldsymbol{\phi}_0+\lambda\boldsymbol{\phi}_1+\lambda^2\boldsymbol{\phi}_2+\ldots+\text{c.c.}, \tag{4.9}$$

where $\lambda=\epsilon^\nu$ for some ν to be determined. Substituting (4.8)–(4.9) into (2.15)–(2.18) yields, by construction, at zeroth order the basic solution: $\boldsymbol{\phi}_0=(1,0,0,0)$. By collecting terms of order-λ we recover the linear problem (at $k=k_c$, $R=R_c$) as was considered in §3. However, there is an essential difference now: ϕ_1 is (also) a function of ξ and τ. Since these two variables do not appear in the linear analysis we find

$$\boldsymbol{\phi}_1(x,y,t,\xi,\tau)=A(\xi,\tau)\boldsymbol{\Phi}_c E_c, \tag{4.10}$$

(compare to (3.12)) for some, up till now, unknown function A (see below for a more detailed discussion). We have to analyse the higher-order systems in order to determine the behaviour of $A(\xi,\tau)$. The nonlinear interactions generate at the second order second harmonics and residual components; however, no extra information on A can be obtained. At third order, the fundamental wave is reproduced by interaction of the fundamental wave itself and the components produced at the second order. This λ^3-component should balance the linear growth of the fundamental wave, which is of order $\epsilon^2\lambda$. Hence we choose $\lambda=\epsilon$, i.e. $\nu=1$. Based upon the observed interaction mechanism between the various harmonics components and on scaling (4.7) we propose the expansion

$$\begin{aligned}\boldsymbol{\phi}(x,y,t,\xi,\tau)=\boldsymbol{\phi}_0 &+\epsilon^2\phi_{02}+\epsilon^3\phi_{03}+\ldots\\ &+E_c[\epsilon\phi_{11}+\epsilon^2\phi_{12}+\epsilon^3\phi_{13}+\ldots]+\text{c.c.}\\ &+E_c^2[\epsilon^2\phi_{22}+\epsilon^3\phi_{23}+\ldots]+\text{c.c.}\\ &+E_c^3[\epsilon^3\phi_{33}+\ldots]+\text{c.c.}\\ &+\ldots,\end{aligned} \tag{4.11}$$

with $\boldsymbol{\phi}_{pq}=\boldsymbol{\phi}_{pq}(\xi,\tau,y)$ describing the response in $O(\epsilon^q,E_c^p)$.

We substitute (4.11) into (2.15)–(2.18) (and take into account (4.1) and (4.8)) and compare equal orders of $\epsilon^qE_c^p$. In general, we will find a set of linear ordinary differential equations of the type

$$\boldsymbol{L}_{pc}\boldsymbol{\phi}_{pq}=\boldsymbol{f}_{pq}\quad\text{where}\quad\boldsymbol{L}_{pc}=\boldsymbol{L}_p|_{\substack{R=R_c\\k=k_c}}, \tag{4.12}$$

with
$$\boldsymbol{L}_p=\begin{pmatrix} p(ik)+2CR & 0 & p(ik) & CR\\ 0 & p(ik)+CR & \dfrac{\partial}{\partial y} & 0\\ p(ik) & \dfrac{\partial}{\partial y} & 0 & -p(ik)\\ p(bik) & \dfrac{\partial}{\partial y} & 0 & p\omega-\dfrac{\gamma}{R}\left(\{p(ik)\}^2+\dfrac{\partial^2}{\partial y^2}\right)\end{pmatrix}, \tag{4.13}$$

and f_{pq} are inhomogeneous terms which depend on ξ, τ and y. They are generated by the nonlinear interactions between the various harmonics and due to the coordinate transformations and the introduction of the 'new' control parameter r. Note that $\boldsymbol{L}_1$ coincides with the linear operator defined in (3.3). This means that $\boldsymbol{L}_{1c}$ is singular. Thus, *a priori*, (4.12) will not be solvable for a general inhomogeneous term f_{1q}: one has to apply a solvability criterion (or Fredholm alternative) in order to solve (4.12) (there are no problems for $p \neq 1$). Applying such a condition at the level $p = 1$, $q = 3$ results in the desired balance between the linear growth and the influence of the nonlinear interactions and yields a nonlinear evolution equation which governs the behaviour of $A(\xi, \tau)$. This equation is known as the Ginzburg–Landau modulation equation.

We shall now discuss equations of the type (4.12) for several values of p and q. We start with $p = 0$, $q = 0$, which leads to the recovering of the basic solution $\boldsymbol{\phi}_0$. The case $p = 1$, $q = 1$ has already been discussed; we recovered the linear problem and, since $f_{11} = 0$ and $\boldsymbol{L}_{1c}$ does not depend on ξ and τ we introduced the amplitude function $A(\xi, \tau)$. Note thus that $\boldsymbol{\phi}_{11} = A(\xi, \tau)\,\Phi_c$, where Φ_c follows from (3.12). The next case we consider is the $O(\epsilon^2)$ residual balance, i.e. $p = 0$, $q = 2$. Note that f_{02} is non-zero since it is generated by interactions between the ϵE_c-mode and its complex conjugate. Because $\boldsymbol{\phi}_{11}$ is already known, it follows that $f_{02} = |A|^2 \tilde{f}_{02}$, for some $\tilde{f}_{02}(y)$ which can be calculated explicitly. It turns out that we have

$$f_{02} = |A|^2 \begin{pmatrix} c_1 \sin^2(\pi y) + c_2 \cos^2(\pi y) \\ c_3 \sin(2\pi y) \\ c_4 \cos(2\pi y) \\ c_5 \cos(2\pi y) \end{pmatrix}. \tag{4.14}$$

Making use of the structure of $\boldsymbol{L}_{0c}$ and f_{02}, we find the solution for $\boldsymbol{\phi}_{02}$:

$$\boldsymbol{\phi}_{02} = |A|^2 \begin{pmatrix} u_{02s} \sin^2(\pi y) + u_{02c} \cos^2(\pi y) \\ v_{02} \sin(2\pi y) \\ \zeta_{02} \cos(2\pi y) \\ z_{02} \cos(2\pi y) \end{pmatrix}. \tag{4.15}$$

The coefficients u_{02c}, u_{02s}, v_{02}, ζ_{02}, z_{02} are functions of $(\alpha_u)_c$, $(\alpha_v)_c$, $(\alpha_\zeta)_c$, k_c and R_c, which are known as asymptotic series in the small parameter δ, defined in (3.11). The final results are presented in Appendix A.

The next case we consider is $p = 2$, $q = 2$, i.e. the second-order and second-harmonic system. This system is forced by nonlinear interactions between the ϵE_c-mode and itself. The analysis of this case is similar to the previous one, i.e. the first-order field $\boldsymbol{\phi}_{11}$ generates the inhomogeneous term f_{22}, which can now be written as

$$f_{22} = A^2 \begin{pmatrix} d_1 \sin^2(\pi y) + d_2 \cos^2(\pi y) \\ d_3 \sin^2(\pi y) \\ d_4 \sin^2(\pi y) + d_5 \cos^2(\pi y) \\ d_6 \sin^2(\pi y) + d_7 \cos^2(\pi y) \end{pmatrix}. \tag{4.16}$$

The solution (4.12) with $p, q = 2$ is of the form

$$\boldsymbol{\phi}_{22} = A^2 \begin{pmatrix} u_{22s} \sin^2(\pi y) + u_{22c} \cos^2(\pi y) \\ v_{22} \sin^2(\pi y) \\ \zeta_{22s} \sin^2(\pi y) + \zeta_{22c} \cos^2(\pi y) \\ z_{22s} \sin^2(\pi y) + z_{22c} \cos^2(\pi y) \end{pmatrix}, \tag{4.17}$$

and substitution results in seven algebraic equations for the seven unknowns in (4.16). The asymptotic results are give in Appendix A.

Now, consider the first harmonic response of the second-order system, i.e. the case $p = 1$, $q = 2$. This results in the equation

$$\boldsymbol{L}_{1c}\boldsymbol{\phi}_{12} = \boldsymbol{f}_{12}. \tag{4.18}$$

Calculations show that $\boldsymbol{f}_{12}$ can be written as follows:

$$\boldsymbol{f}_{12} = \mathrm{i}\left(\frac{\partial \boldsymbol{L}_1}{\partial k}\right)_c \frac{\partial \boldsymbol{\phi}_{11}}{\partial \xi} = \mathrm{i}\frac{\partial A}{\partial \xi}\left(\frac{\partial \boldsymbol{L}_1}{\partial k}\right)_c \boldsymbol{\Phi}_c. \tag{4.19}$$

Note that in this case $\boldsymbol{f}_{12}$ is generated due to the coordinate transformation introduced in (4.7) and therefore contains only first-order derivatives with respect to the slow spatial coordinate ξ, i.e. $\boldsymbol{f}_{12} = (\partial A/\partial \xi)\tilde{\boldsymbol{f}}_{12}$, for some $\tilde{\boldsymbol{f}}_{12}(y)$. We now make the following observation: consider the general linear problem (3.2)–(3.3), which in the context of this section can also be written as

$$\boldsymbol{L}_1 \boldsymbol{\Phi} = 0. \tag{4.20}$$

Differentiation of (4.20) with respect to k and evaluation in $k = k_c$, $R = R_c$ yields

$$\left(\frac{\partial \boldsymbol{L}_1}{\partial k}\right)_c \boldsymbol{\Phi}_c + \boldsymbol{L}_{1c}\left(\frac{\partial \boldsymbol{\Phi}}{\partial k}\right)_c = 0. \tag{4.21}$$

This observation can be used to find a solution for the problem $\boldsymbol{L}_{1c}\boldsymbol{\phi}_{12} = \boldsymbol{f}_{12}$. Equation (4.18) can be reformulated as

$$\boldsymbol{L}_{1c}\boldsymbol{\phi}_{12} = -\mathrm{i}\frac{\partial A}{\partial \xi}\boldsymbol{L}_{1c}\left(\frac{\partial \boldsymbol{\Phi}}{\partial k}\right)_c, \tag{4.22}$$

with the solution

$$\boldsymbol{\phi}_{12} = \boldsymbol{\phi}_{12p} + \boldsymbol{\phi}_{12h}, \tag{4.23}$$

where

$$\boldsymbol{\phi}_{12p} = -\mathrm{i}\frac{\partial A}{\partial \xi}\left(\frac{\partial \boldsymbol{\Phi}}{\partial k}\right)_c \quad \text{and} \quad \boldsymbol{L}_{1c}\boldsymbol{\phi}_{12h} = 0.$$

Note that $\boldsymbol{\phi}_{12p}$ is a known particular solution, whereas the homogeneous solution is given by $\boldsymbol{\phi}_{12h} = A_2(\xi, \tau)\boldsymbol{\Phi}_c$, with a second, unknown amplitude function A_2. This second amplitude function is a result of the application of the Fredholm alternative where the solvability condition on this level is automatically satisfied by $\boldsymbol{f}_{12}$ (essentially this is a consequence of our 'choice' to move with the group velocity v_k, see (4.7)). We have to introduce A_2 as a consequence of the non-uniqueness of the solution as provided by the Fredholm alternative and it should be noted that A_2 is unimportant for the subsequent analysis. Owing to the structure of expansion we will meet at any level of the analysis this type of 'solvability' behaviour.

The final case we consider is $p = 1$, $q = 3$, i.e.

$$\boldsymbol{L}_{1c}\boldsymbol{\phi}_{13} = \boldsymbol{f}_{13} \equiv \boldsymbol{f}_{13,\,\mathrm{lin}} + \boldsymbol{f}_{13,\,\mathrm{nonlin}}. \tag{4.24}$$

Here, $\boldsymbol{f}_{13,\,\mathrm{lin}}$ contains terms which are linear in the amplitude A, whereas $\boldsymbol{f}_{13,\,\mathrm{nonlin}}$ contains all the nonlinear terms. It turns out that the linear terms in $\boldsymbol{f}_{13}$ can be written as

$$\boldsymbol{f}_{13,\,\mathrm{lin}} = \boldsymbol{M}\boldsymbol{\phi}_{12} + \boldsymbol{N}\boldsymbol{\phi}_{11}, \tag{4.25}$$

where

$$\boldsymbol{M} = \mathrm{i}\frac{\partial}{\partial \xi}\left(\frac{\partial \boldsymbol{L}_1}{\partial k}\right)_c; \quad \boldsymbol{N} = \left\{-r\frac{\partial \boldsymbol{L}_1}{\partial R} + \frac{1}{2}\frac{\partial^2}{\partial \xi^2}\frac{\partial^2 \boldsymbol{L}_1}{\partial k^2}\right\}_c + \boldsymbol{S}, \tag{4.26}$$

and $\boldsymbol{S}$ is a 4×4 matrix with all elements zeros, except

$$\boldsymbol{S}(4,4) = -\frac{\partial}{\partial\tau} + r\left(\frac{\partial\omega}{\partial R}\right)_c - \frac{1}{2}\left(\frac{\partial^2\omega}{\partial k^2}\right)_c \frac{\partial^2}{\partial\xi^2}. \tag{4.27}$$

Substituting (4.25)–(4.27) in (4.24) and using (4.20) to evaluate the derivatives of $\boldsymbol{L}$ with respect to k and R results in

$$\boldsymbol{L}_{1c}\boldsymbol{\phi}_{13} = \boldsymbol{f}_{13} = \boldsymbol{L}_{1c}\left[-\frac{1}{2}\frac{\partial^2 A}{\partial\xi^2}\left(\frac{\partial^2\boldsymbol{\Phi}}{\partial k^2}\right) - \mathrm{i}\frac{\partial A_2}{\partial\xi}\frac{\partial\boldsymbol{\Phi}}{\partial k} + r\frac{\partial\boldsymbol{\Phi}}{\partial R}\right]_c + \boldsymbol{S}\boldsymbol{\phi}_{11} + \boldsymbol{f}_{13,\,\mathrm{nonlin}}. \tag{4.28}$$

In the derivation of (4.28), we have used a same kind of reasoning as in the case of $p = 1$, $q = 2$, where (4.18) was rewritten as (4.22). In the present case we have used the differentiation of (4.20) with respect to R, as well as the second-order derivative of (4.20) with respect to k. We must apply the Fredholm alternative to the right-hand side of (4.28). This means that we have to determine

$$\langle \boldsymbol{f}_{13}, \boldsymbol{\Phi}_c \rangle = \int_0^1 \boldsymbol{f}_{13}\,\boldsymbol{\Phi}_c^{\mathrm{A}}\,\mathrm{d}y = 0,$$

where $\boldsymbol{\Phi}_c^{\mathrm{A}}$ are the eigenfunctions of the adjoint linear problem at critical conditions. To avoid calculation of the eigenfunctions of the adjoint problem, we again reduce problem (4.28) to one equation for $\phi_{13}^{(4)}$, where $\phi_{13}^{(4)}$ is the fourth component of the vector $\boldsymbol{\phi}_{13}$, in which case the eigenfunctions (i.e. $\sim\cos(p\pi y)$) coincide with their adjoints. Note however that, in applying the Fredholm alternative, the first term in the right-hand side of (4.28) vanishes, and thus $\boldsymbol{S}\boldsymbol{\phi}_{11}$ is the only contribution to the linear terms when we evaluate the inner product. We observe that the reduced problem can be written as $L\phi_{13}^{(4)} = \tilde{g}$, where L follows from (3.5) and $\tilde{g}$ reads:

$$\begin{aligned}\tilde{g} = {} & -k_c^2(\mathrm{i}k_c + CR_c)[f_{13}^z - f_{13}^\zeta] + (\mathrm{i}k_c + 2CR_c)\frac{\partial^2}{\partial y^2}[f_{13}^z - f_{13}^\zeta] \\ & - \mathrm{i}k_c(b-1)\frac{\partial^2}{\partial y^2}f_{13}^u - (b-1)\,k_c^2\frac{\partial}{\partial y}f_{13}^v + k_c^2(b-1)\,(\mathrm{i}k_c + CR_c)f_{13}^\zeta.\end{aligned} \tag{4.29}$$

The components $f_{13}^{(i)}$ of the vector $\boldsymbol{f}_{13}$ can be found in Appendix B. Tedious calculations then show that

$$\tilde{g} = g_1(y) + g_2\cos(\pi y) + |A|^2 A(g_3\cos(\pi y)\sin^2(\pi y) + g_4\cos^3(\pi y)). \tag{4.30}$$

For $g_1, \ldots, g_4$ refer again to Appendix B. The Fredholm alternative reads in this case

$$\langle \tilde{g}(y), \cos(\pi y)\rangle = \int_0^1 \tilde{g}(y)\cos(\pi y)\,\mathrm{d}y = 0. \tag{4.31}$$

Evaluating expression (4.31) finally leads to a nonlinear partial differential equation for the amplitude A:

$$\frac{\partial A}{\partial\tau} = r(\tau_r + \mathrm{i}\nu_r)A - \tfrac{1}{2}(\tau_{k^2} + \mathrm{i}\nu_{k^2})\frac{\partial^2 A}{\partial\xi^2} + (c_r + \mathrm{i}c_i)|A|^2 A. \tag{4.32}$$

This modulation equation, the so-called Ginzburg–Landau equation, governs all the pattern generating processes. The evolution of a pattern, whether it is periodic or non-periodic (see §5), is always determined by the timescale τ and the spatial scale ξ (see (4.7)). Thus, the timescale on which a solution of (4.32) develops into a stable pattern

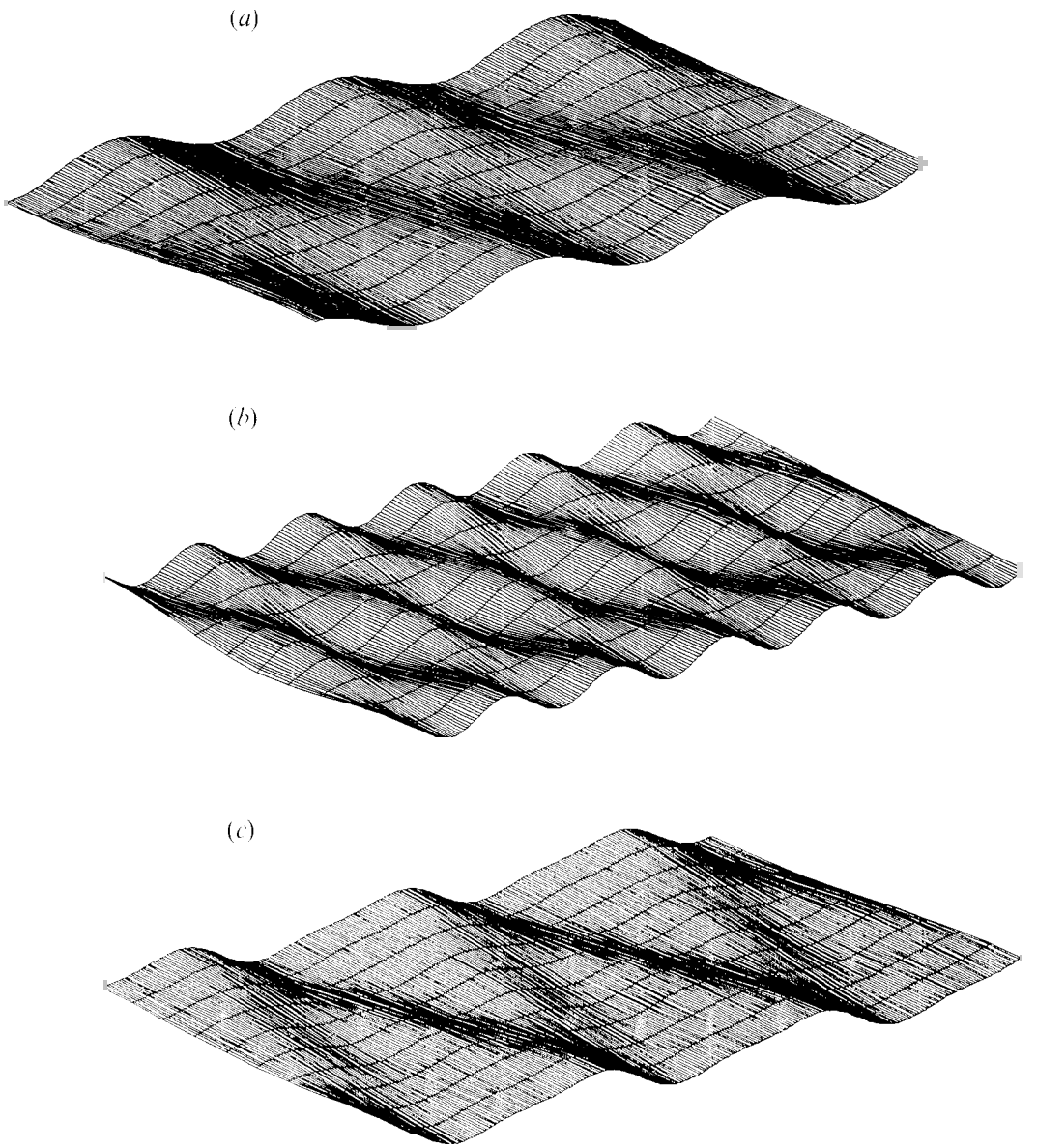

FIGURE 3. Approximations at various order of the bed profile as described by (4.11). Solutions up to $O(\epsilon)$ are known in terms of the parameters δ, ϵ and the amplitude A. On the short spatial scale visualized here, the amplitude may be considered as a constant, which is yet unspecified. Here we have taken $b = 5$, $C = 0.007$, $\gamma = 1$, $\epsilon = 0.35$ and $A = 1$. (*a*) The $O(\epsilon)$ approximation of the bed profile, i.e. the linear wave solution at critical conditions. (*b*) The nonlinear $O(\epsilon^2)$ correction on the linear profile. (*c*) The $O(\epsilon^2)$ approximation of nonlinear bed profile. This is the superposition of the two profiles shown in (*a*) and (*b*). Note the steep wave fronts and the flat wakes caused by the phase difference between the linear profile and the nonlinear $O(\epsilon^2)$ correction.

does not depend on the complexity of this pattern. Furthermore, if (4.32) has no stable periodic solutions (see § 5), then any initial pattern will immediately (on the τ-timescale) evolve to a non-periodic pattern: an observer will not see a first (time-)step in which the initial pattern becomes periodic and a second step in which this periodic pattern is slowly (in τ) modulated into a non-periodic pattern.

Note that the coefficients of the linear terms follow from the expansion for ω (see also (4.4)). For asymptotic results for the coefficients of (4.32) refer to Appendix B. It should be remarked here that c_r is smaller than zero (for physically interesting values of b, γ and C). In terms of the Ginzburg–Landau equation it means that the exponential growth governed by the linear part is counteracted by nonlinear effects, so we may expect finite-amplitude solutions.

At this point in the theory the expressions for $\boldsymbol{\phi}_{11}$, $\boldsymbol{\phi}_{02}$, $\boldsymbol{\phi}_{12}$ and $\boldsymbol{\phi}_{22}$ are known in terms of the model parameters. Thus, we are able to visualize the nonlinear bed profile, using (4.11), for an, at this time, undetermined amplitude. A typical result is shown in figure 3. Individual waves move with the phase velocity $|\mathrm{i}\omega/k|$, where k satisfies (4.2). On the other hand, the energy of the wave group moves with the group velocity $|\nu_k|$ (for an asymptotic expression for ν_k, see Appendix B). In turns out that $|\mathrm{i}\omega/k| > |\nu_k|$ where k satisfies (4.2), i.e. the group velocity is larger than the phase velocity. This phenomenon is called anormal dispersion.

5. Analysis of the Ginzburg–Landau equation

In this section we shall present some properties of the Ginzburg–Landau equation which are relevant for our morphological model. At first, we consider the possibility of periodic solutions. We shall give conditions for the stability of these solutions and give predictions of their (finite) amplitude and phase.

We consider periodic solutions of the following form:

$$A(\xi,\tau) = G\,\mathrm{e}^{\mathrm{i}(K\xi+W\tau)} \quad \text{with} \quad G, K, W \in R. \tag{5.1}$$

Note that periodic solutions of this type correspond to the bifurcating unstable waves (the alternate bars) of the linearized theory and also appear in the Landau theory (however, then K is fixed, here it is a parameter). The solution with $K = 0$ is called the Stokes wave. Substitution of (5.1) in (4.32) and splitting the expression into real and imaginary parts yields

$$0 = r\tau_r + \tfrac{1}{2}K^2\tau_{k^2} + G^2 c_r, \tag{5.2}$$

$$W = r\nu_r + \tfrac{1}{2}K^2\nu_{k^2} + G^2 c_i. \tag{5.3}$$

Equation (5.2) gives, for every choice of K and r, the amplitude and the shift in phase (with respect to the critical wave) of the periodic solutions (i.e. the amplitude and the phase of the free bars). We use the periodic solutions (5.1) of the Ginzburg–Landau equation where K, G and W follow from (5.2)–(5.3) in order to find an expression for the bottom evolution z_b. Applying (4.11) yields

$$\begin{aligned} z_b &= \epsilon A(\xi,\tau)\,\mathrm{e}^{\mathrm{i}k_c x+\omega_c t}\cos(\pi y) + \ldots + \text{c.c.} \\ &= \epsilon G \exp[\mathrm{i}(k_c+\epsilon K)x + (\omega_c + \mathrm{i}\epsilon\nu_k K + \mathrm{i}\epsilon^2 W)\,t]\cos(\pi y) + \ldots + \text{c.c.} \end{aligned} \tag{5.4}$$

Thus, in this case, the fundamental wave is modulated, where the modulation is expressed in an $O(\epsilon)$ change in the critical wavenumber and an $O(\epsilon^2)$ change in the critical frequency. Note that (5.2) represents (half) an ellipse in the (K, G)-plane for $r > 0$. This is due to the signs of τ_r, τ_{k^2} and c_r (see Appendix B). Thus, periodic solutions only exist for $r > 0$, i.e. $R > R_c$, which agrees with the linear predictions. Figure 4 is a contour plot of the maximal amplitude which is reached at $K = 0$, i.e. at $k = k_c$. Note that it can be seen from (5.2) that increasing r leads to increasing amplitude G. To find the maximal amplitude, we have set $r = R_c$, as is motivated by (4.1). It appears that our predicted amplitudes are slightly larger than those obtained from the model of Colombini *et al.* (1987). A reasonable comparison is expected to be possible if we

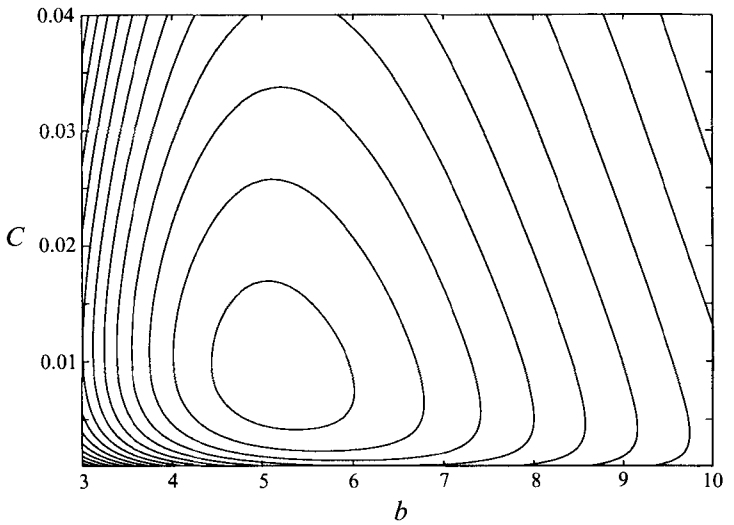

FIGURE 4. A contour plot of the maximal amplitude of the Stokes wave, as determined by (5.2), in the b, C parameter space for $\gamma = 1$ and $r = R_c$, where R_c is defined in (3.16). The contour line in the middle corresponds to a maximal amplitude of 0.54. The distance between the contour lines is 0.01.

choose $b = 3$, $\gamma = 1$ and C between 0.002 and 0.003, which implies that free surface effects in the latter model are negligible. In this case we obtain amplitudes of order 0.4 whereas Colombini *et al.* (1987) report values of order 0.3. These differences are because their model includes the variation of the drag coefficient with the local water depth, the presence of a critical shear stress for erosion and the dependence of the bed slope correction coefficient on the bottom shear stress. On the other hand, slightly larger amplitudes are not unrealistic since the results of Colombini *et al.* (1987) show more under- than overestimation of observed alternate bar amplitudes.

We remark that (5.3) is again a dispersion relation. Since the coefficient c_i is positive (see Appendix B), it can be seen from (5.3) that the frequency W increases with increasing amplitude. This means that the total frequency of the alternate bars, which is $|-i\omega_c + \epsilon\nu_k K + \epsilon^2 W|$, decreases if the amplitude becomes larger or, in other words, the nonlinear bars move slower than is predicted by linear theory. This is a general property of anormal dispersive waves.

The periodic solutions obtained so far are also found by standard Landau theory, in which case they are always stable (Colombini *et al.* 1987). In our model, interactions between various wave components can cause the basic periodic solution (5.1) to become unstable. In order to investigate this possibility, we consider a general perturbation of a periodic solution of the type (5.1):

$$A(\xi,\tau) = [G+\rho(\xi,\tau)]\,\mathrm{e}^{\mathrm{i}(K\xi+W\tau+\theta(\xi,\tau))}. \tag{5.5}$$

Inserting (5.5) into (4.32) and using (5.2) and (5.3) to simplify intermediate results yields after linearizing

$$\rho_\tau = r\tau_r\rho + \tfrac{1}{2}|\tau_{k^2}|\,(\rho_{\xi\xi} - 2GK\theta_\xi - K^2\rho) + \tfrac{1}{2}\nu_{k^2}(2K\rho_\xi + G\theta_{\xi\xi}) - 3|c_r|\,G^2\rho \tag{5.6}$$

$$G\theta_\tau = -W\rho + r\nu_r\rho + \tfrac{1}{2}|\tau_{k^2}|\,(2K\rho_\xi + G\theta_{\xi\xi}) - \tfrac{1}{2}\nu_{k^2}(\rho_{\xi\xi} - 2GK\theta_\xi - K^2\rho) + 3c_i\,G^2\rho. \tag{5.7}$$

Owing to the structure of these linear equations we may assume

$$\rho(\xi,\tau) = X(\tau)\,\mathrm{e}^{\mathrm{i}l\xi}, \tag{5.8}$$

$$G\theta = Y(\tau)\,\mathrm{e}^{\mathrm{i}l\xi}, \tag{5.9}$$

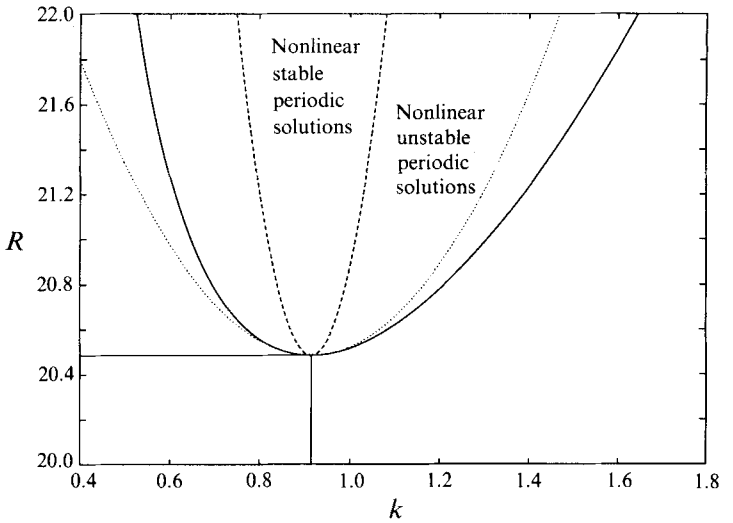

FIGURE 5. Neutral curve with inner parabola for the case $b = 5$, $C = 0.007$ and $\gamma = 1$. The dotted line is the second-order approximation of the neutral curve which is represented as a solid line. The dashed line is the boundary of the stable area from the nonlinear point of view.

with an arbitrary wavenumber $l \in R$. Substitution of (5.8)–(5.9) into (5.6)–(5.7), and using (5.2)–(5.3) we get rid of terms containing W and K^2, leads to

$$\frac{\mathrm{d}}{\mathrm{d}\tau}\begin{pmatrix} X \\ Y \end{pmatrix} = \begin{pmatrix} -\frac{1}{2}l^2|\tau_{k^2}| + \mathrm{i}\nu_{k^2} lK - 2|c_r| G^2 & -\frac{1}{2}l^2\nu_{k^2} - \mathrm{i}lK|\tau_{k^2}| \\ \frac{1}{2}l^2\nu_{k^2} + \mathrm{i}lK|\tau_{k^2}| + 2c_i G^2 & -\frac{1}{2}l^2|\tau_{k^2}| + \mathrm{i}lK\nu_{k^2} \end{pmatrix}\begin{pmatrix} X \\ Y \end{pmatrix}. \tag{5.10}$$

The stability of a general periodic solution of type (5.1) of the Ginzburg–Landau equation is now reduced to the stability of the zero-solution in the (X, Y)-system, a linear 2×2 matrix equation. Hence, we compute the eigenvalues of this matrix and impose the condition that the real parts of both eigenvalues have to be negative for all l. This yields, after tedious calculations, a condition on K^2:

$$K^2 \leqslant \frac{r\tau_r|c_r|\,(|c_r|\,|\tau_{k^2}| + c_i\,\nu_{k^2})}{\frac{3}{2}|\tau_{k^2}|^2\,|c_r|^2 + |\tau_{k^2}|^2\,c_i^2 + \frac{1}{2}|\tau_{k^2}|^2\,\nu_{k^2}|c_r|\,c_i}. \tag{5.11}$$

For more details on the stability analysis of periodic solutions of the Ginzburg–Landau equation, we refer to Stuart & DiPrima (1978) or to Matkowski & Volpert (1993). Expression (5.11) gives a bandwidth in which one can expect finite-amplitude solutions. The condition on K defines an 'inner-parabola' in the neutral curve in which periodic solutions are stable with respect to general perturbations. Figure 5 is a plot of the neutral curve with inner parabola, for a fixed value of δ (see (3.11)). Note that whenever

$$\chi = |c_r|\,|\tau_{k^2}| + c_i\,\nu_{k^2} < 0 \tag{5.12}$$

(5.11) cannot be satisfied for any K. This means that all periodic solutions of the type (5.1) are unstable. In figure 5 it means that the inner parabola vanishes at $K = 0$, thus the Stokes wave is the last periodic solution to become unstable.

A physical explanation of this stability criterion has been given by Lighthill (1978). Consider a slowly modulated Stokes wave, the amplitude of which is described by (4.32). The bedforms will have their largest elevations at the top of the envelope wave. Since $c_i > 0$ in our model, the dispersion relation (5.3) implies that the phase velocity

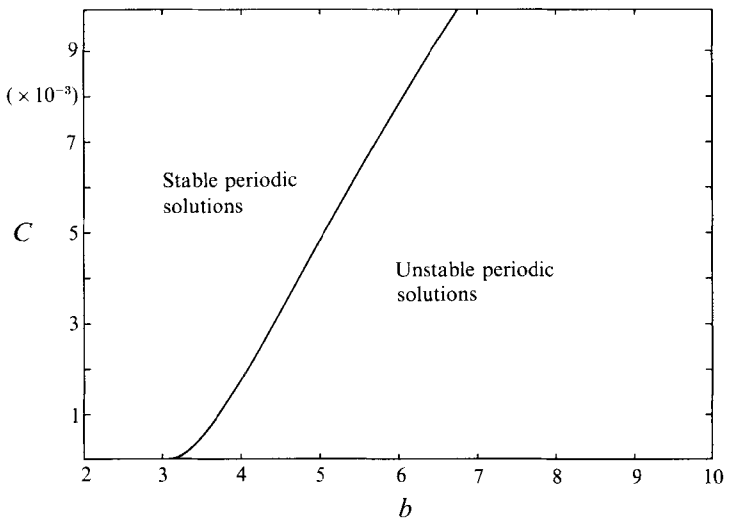

FIGURE 6. The neutral stability curve $\chi = 0$ (χ is defined in (5.12)), for periodic bar patterns of the type (5.1) in the b, C parameter space for $\gamma = 1$, in the case of a continuous model. To the left of this curve, standard Landau theory yields valid results while in the other region different bed profiles are to be expected.

at the top is smaller than at either side. Consequently, the bedforms on the downstream side are enlarged whereas the waves at the upstream sides are shortened. A necessary condition for instabilities to occur is that there will be an accumulation of energy at the top. Since energy is transported by the group velocity ν_k, this requires in the present model $\partial|\nu_k|/\partial k > 0$ or, in other words, $\nu_{k^2} < 0$. This is precisely what is determined by condition (5.12).

The computations give analytical results on the stability, i.e. existence in physical sense, of the alternate bars (periodic solutions (5.1)). Stability interval (5.11) and, maybe more important, condition (5.12) can be derived from the fact that the Ginzburg–Landau theory admits spatial variation. The Landau theory can only predict the stability of an alternate bar with respect to very special perturbations (those with exactly the same wavenumber as the bar), which for instance yields that all alternate bars are stable. Hence, the non-existence of stable alternate bars (condition (5.12)) cannot be predicted by the Landau theory. In figure 6 we plot the expression $\chi = 0$ for $0.001 \leqslant C \leqslant 0.01$ and for $2 \leqslant b \leqslant 10$ while $\gamma = 1$. It is readily observed that the physically interesting domain for C and b contains combinations of the parameters where we can expect stable periodic solutions as well as combinations where the instability criterion (5.12) is satisfied, i.e. where the periodic solutions are not stable. From figure 6 we can conclude that for $b < 3$, the periodic bar pattern as predicted by the Landau theory (Colombini *et al.* 1987) is stable, while for $b > 3$, i.e. when the bed is dune covered, more complicated bed profiles may be expected, depending on the value for C. Thus, within the natural parameter region there is a change from existence to non-existence of stable alternate bars. It should be noted (again), that, due to the character of evolution equation (4.32), there is no transient behaviour between a periodic and a non-periodic pattern when instability criterion (5.12) is satisfied: any initial solution will immediately evolve to a non-periodic pattern, without becoming periodic first.

We will use some numerical techniques in order to study the evolution of solutions of the Ginzburg–Landau equation when all periodic solutions are unstable. First, we

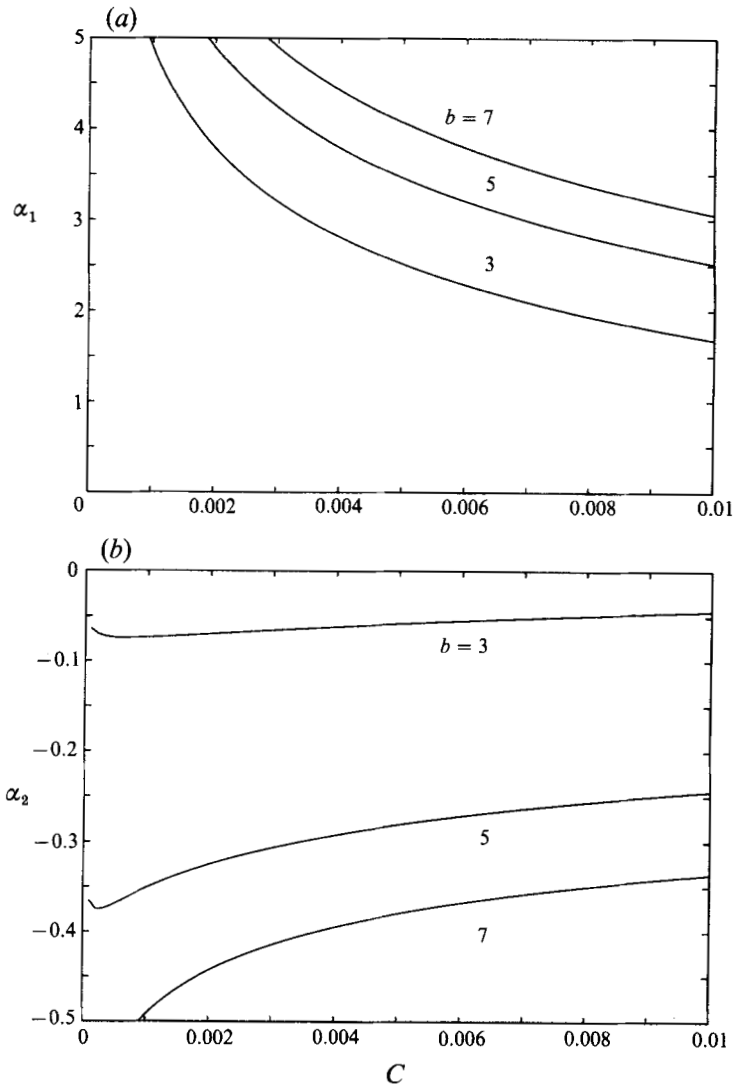

FIGURE 7. The coefficients (*a*) α_1 and (*b*) α_2 of the rescaled Ginzburg–Landau equation (5.14), as function of C for several values of b when $\gamma = 1$.

bring equation (4.32) into a standard form (as is done in Doelman 1991; Doering *et al.* 1988; Keefe 1985). Substitution of

$$A = DA'(\xi', \tau')\,\mathrm{e}^{r\mathrm{i}\nu_r\tau'} \tag{5.13}$$

in (4.32), where $D^2 = \dfrac{-r\tau_r}{c_r}$, $\tau = \dfrac{1}{r\tau_r}\tau'$, $\xi = \left(\dfrac{-2r\tau_r}{\tau_{k^2}}\right)^{\frac{1}{2}}\xi'$,

yields the rescaled Ginzburg–Landau equation (primes are dropped for convenience)

$$\frac{\partial A}{\partial \tau} = A + (1+\mathrm{i}\alpha_1)\frac{\partial^2 A}{\partial \xi^2} - (1+\mathrm{i}\alpha_2)|A|^2 A \tag{5.14}$$

with $\alpha_1 = \nu_{k^2}/\tau_{k^2}$; $\alpha_2 = c_i/c_r$. Plots of α_1 and α_2 are given in figure 7. We cannot choose α_1 and α_2 arbitrary, as is done in some theoretical studies. They are determined by our

model parameters and it appears that we end up with pairs (α_1, α_2) that have not been studied in the context of the Ginzburg–Landau equation before. Because the Stokes wave is the last wave to become unstable, and we are interested in bifurcating solutions from this last stable wave, it is natural to perform a stability analysis around the Stokes wave. Repeating the above general stability analysis for the special case of the Stokes wave, which now corresponds to $\exp(-i\alpha_2\tau)$, for the scaled equation (5.14), we find

$$\frac{d}{d\tau}\begin{pmatrix} X \\ Y \end{pmatrix} = \begin{pmatrix} -2-l^2 & l^2\alpha_1 \\ -2\alpha_2-\alpha_1 l^2 & -l^2 \end{pmatrix}\begin{pmatrix} X \\ Y \end{pmatrix}, \tag{5.15}$$

the analogue of (5.10), and the Stokes wave is stable if perturbations of the type (5.5) decay exponentially, i.e. if the eigenvalues of (5.15) are smaller than zero. This leads to a condition on l: the Stokes wave is stable against perturbations with wavenumbers l satisfying

$$|l| \geqslant l_c = \left(\frac{-2(1+\alpha_1\alpha_2)}{1+\alpha_1^2}\right)^{\frac{1}{2}}, \tag{5.16}$$

i.e. perturbations with a small wavenumber are the most unstable ones (this has already been observed by Benjamin & Feir 1967; Stuart & DiPrima 1978). Note that the Stokes wave is stable against all perturbations if $1+\alpha_1\alpha_2 > 0$; $1+\alpha_1\alpha_2 < 0$ is the rescaled version of (5.12).

Since we cannot apply numerical methods to (5.14) on an unbounded domain, we restrict ξ to an interval $[0, 2\pi/q]$ and consider no-flux boundary conditions (i.e. $\partial A/\partial\xi = 0$ at $\xi = 0, 2\pi/q$). Physically this means that we cut the infinitely straight channel into periodic parts of length $2\pi/q$. The boundary conditions are introduced mainly for convenience, they are of no essential significance to our problem. We can use the spectral method also discussed in Keefe (1985) and Doelman (1991) and introduce

$$A(\xi, \tau) = \sum_{n=-\infty}^{\infty} Z_n(\tau)\, e^{inq\xi}. \tag{5.17}$$

Note that $Z_n = Z_{-n}$, which is a result of the boundary conditions, and that q corresponds directly to the l in the stability analysis. By decreasing q we introduce solutions (and thus perturbations) with small wavenumbers l to the interval $[0, 2\pi/q]$. In other words, the Stokes wave is a stable solution of the Ginzburg–Landau equation on the interval $[0, 2\pi/q]$ (with no-flux boundary conditions) if $q > q_c = l_c$ where l_c is defined in (5.16) (for more details, see Doelman 1991). In figure 8 a contour plot is shown of l_c^2 in the (b, C) parameter space for $\gamma = 1$. From this it can be seen that for realistic combination of these parameters the critical value $q = q_c$ ranges between 0 and 0.32. Note that $2\pi/q_c$ is the minimum interval length necessary for observing modulations of the Stokes wave as solutions of the rescaled Ginzburg–Landau equation (5.14). Using (4.6) and (5.13) we define the minimum modulation length for the unscaled Ginzburg–Landau equation (4.32) as

$$L_c = \frac{2\pi}{q_c}\left(\frac{\frac{1}{2}\tau_{k^2}}{\epsilon_r^2\tau_r}\right)^{\frac{1}{2}} \tag{5.18}$$

in units of channel width. Actual values for L_c strongly depend on the value of ϵ. As we have already discussed we expect the weakly nonlinear theory to yield valid results even if ϵ becomes of order 1. Consequently, typical values for L_c range from several tens to a few hundred channel widths, which do not seem unrealistically large. In our

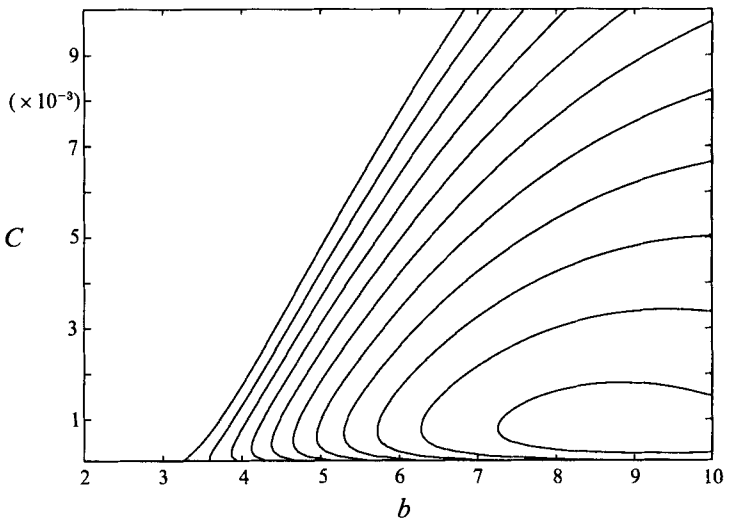

FIGURE 8. A contour plot of l_c^2 (where l_c is defined in (5.16)) in the b, C parameter space for $\gamma = 1$. Here l_c corresponds to a critical value q_c for the parameter q (the smallest resolved wavenumber) in the spectral model, below which the Stokes wave is unstable. Note that the contour line $l_c^2 = 0$ coincides with the curve $\chi = 0$ of the continuous model, as presented in figure 6. The distance between the contour lines is 0.01.

experiments we considered $q \geqslant 0.05$ such that the channel lengths were less than approximately $300/\epsilon$ width units.

Note that any initial perturbation of the flat bed evolves on an $O(1/\epsilon^2)$ timescale to a fully developed periodic or quasi-periodic bed profile. During this transient behaviour, the envelope amplitude propagates with an $O(1)$ group velocity ν_k, which means that we would actually need a channel with a length of the order $1/\epsilon^2$ and not of the order of $1/\epsilon$ as is suggested by L_c (see (5.18)). Therefore, a realistic indication of the minimum channel length necessary for actually observing a quasi-periodic modulation behaviour is given by L_c/ϵ. A consequence of this observation is that, if we want to detect the predicted bed profiles in laboratory or field conditions, we are obliged to choose ϵ not too small. Otherwise, the length needed in a laboratory or the length of a straight natural river as predicted by our theory (i.e. $O(1/\epsilon^2)$) will become unrealistically large.

By substituting (5.17) into (5.14) one analyses the stability of the Stokes wave ($Z_0(\tau) = \exp(-i\alpha_2\tau), Z_n(\tau) = 0, n \neq 0$), because the terms $\exp(inq\xi)$ are perturbations to which the Stokes wave eventually (i.e. by sufficiently small q) will become unstable. Hence, it is natural to consider q as a bifurcation parameter in the subsequent analysis. Performing the former substitution yields an ∞-dimensional system of nonlinear coupled differential equations and truncating at a finite dimension N yields a Galerkin approximation:

$$\frac{\mathrm{d}}{\mathrm{d}\tau} Z_n^N = (1 - n^2 q^2 (1 + i\alpha_1)) Z_n + (1 + i\alpha_2) \sum_{\substack{k+l+m<N \\ |k|,\,|l|,\,|m|<N}} Z_k Z_l Z_m. \tag{5.19}$$

We consider (5.19) with $N = 3$ as approximating system of (5.14) (i.e. a 4-dimensional complex or a 8-dimensional real system). This choice is motivated by experiments of Doelman (1991) who investigated more thoroughly system (5.19) and found no significant difference in the dynamics of the system when truncated at $N = 3$, and at

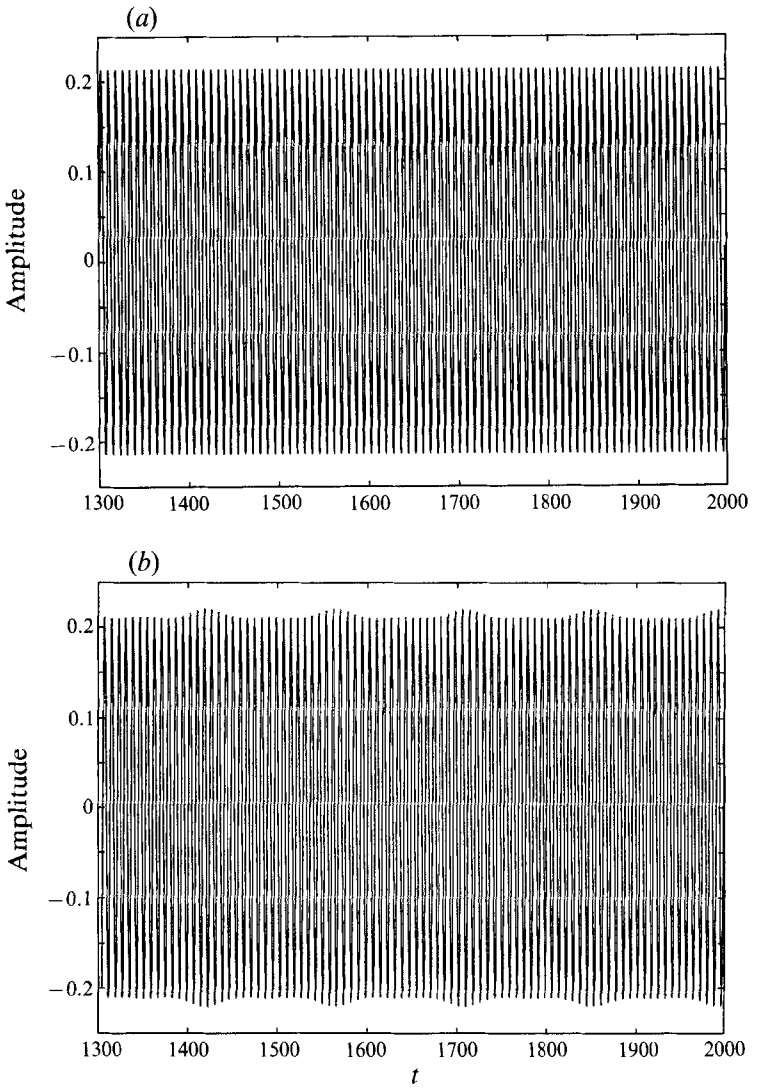

FIGURE 9 (*a*, *b*). For caption see facing page.

$N = 31$, which was studied by Keefe (1985). In the numerical simulation of system (5.19), we fixed the morphological parameters b, C, γ and $\epsilon^2 r$ and computed the coefficients α_1 and α_2 in (5.14) using the asymptotic expressions presented in Appendix B. The corresponding bed profile, as given by (4.11), becomes

$$\begin{aligned} z_b &= \epsilon A(\xi,\tau)\,\mathrm{e}^{\mathrm{i}k_c x+\omega_c t}\cos(\pi y)+\ldots+\text{c.c.} \\ &= \epsilon D\sum_{n=-N}^{N}\hat{Z}_n(t)\,\mathrm{e}^{\mathrm{i}(C_{1n}x+C_{2n}t)}\cos(\pi y)+\ldots+\text{c.c.}, \end{aligned} \tag{5.20}$$

where D follows from (5.13), $\hat{Z}_n(t) \equiv Z_n(\epsilon^2 r\tau_r t)$ and

$$C_{1n} = \epsilon nq\left(\frac{\tau_{k^2}}{-2r\tau_r}\right)^{\frac{1}{2}}+k_c, \tag{5.21}$$

$$C_{2n} = \epsilon^2 r^2\tau_r\nu_r+\epsilon nq\nu_k\left(\frac{\tau_{k^2}}{-2r\tau_r}\right)^{\frac{1}{2}}-|\omega_c|. \tag{5.22}$$

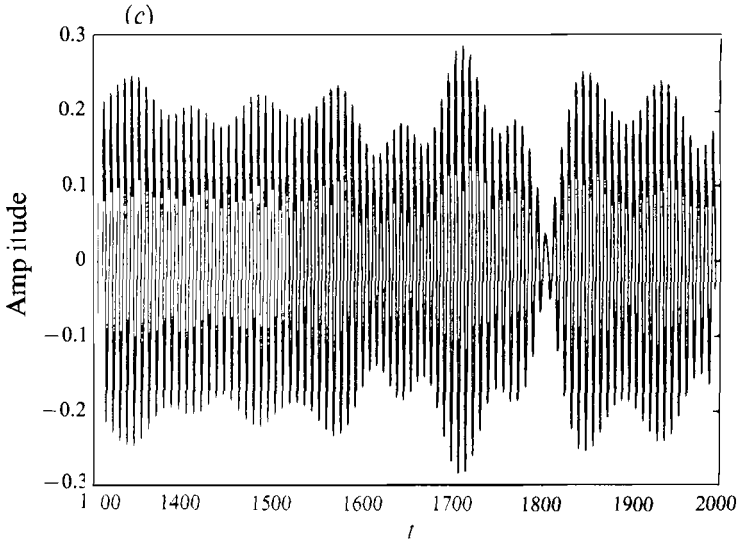

FIGURE 9. Long-term behaviour of the bed profile (at a fixed position near the channel bank) as a function of the dimensionless time t. In the numerical simulations we have set $b = 6$, $C = 0.003$, $\gamma = 1$, $r = R_c = 26.91$ and $\epsilon = 0.2$. (*a*) $q = 0.28$, which is larger than the critical value $q_c = 0.2556$. The solution of the spectral model is a Stokes wave, resulting in a regular oscillatory bed profile. (*b*) $q = 0.2$, which is between q_c and $q_H = 0.1168$. The spectral model has a periodic solution where all components Z_n have finite, non-zero amplitude. As follows from (5.20), the behaviour of the bed is quasi-periodic with two fundamental frequencies. (*c*) $q = 0.1 < q_H$. Solutions of the spectral model are quasi-periodic with two fundamental frequencies, resulting in quasi-periodic bed evolution with three fundamental frequencies.

Here, use has been made of definition (4.7), transformation (5.13) and representation (5.17).

Experiments with $q > q_c = l_c$ (see (5.16)) demonstrated that in these cases, solutions of the spectral model converge to a stable Stokes wave, for which

$$Z_0(t) = \exp(-i\alpha_2 \epsilon^2 r \tau_r t)$$

and $\hat{Z}_n(t) = 0$ for $n \neq 0$. According to (5.20), this describes a periodic alternate bar pattern. The corresponding bed profile, at a fixed position of the bank of the channel, as a function of the dimensionless time t is shown in figure 9(*a*). At $q = q_c$, the Stokes wave becomes unstable, due to a pitchfork bifurcation. For slightly smaller q-values, two new periodic solutions with $\hat{Z}_n(t) \neq 0$ for all n are observed. From (5.20) it follows that, in this case, the bed profile is composed of a series of travelling waves, each with their own wavenumber and frequency. It appears that all frequencies of this solution follow from integer combinations of two fundamental frequencies which are mutually irrational. Consequently, the temporal and spatial behaviour of the bar pattern is quasi-periodic, even though the solutions of the spectral model are periodic. An example of the bed evolution for such a situation at a fixed position near the bank as a function of time is shown in figure 9(*b*). If q is further decreased, the two periodic attractors become unstable due to a Hopf bifurcation at the critical value $q = q_H$. Solutions of the spectral model are then themselves quasi-periodic with two fundamental frequencies. As a consequence of (5.20), the bed profile become quasi-periodic with three independent frequencies. An example of the corresponding bed profile is shown in figure 9(*c*). As can be seen from (5.20)–(5.22), the bed pattern is not only quasi-periodic in time, but also in space. This behaviour is visualized in figure 10,

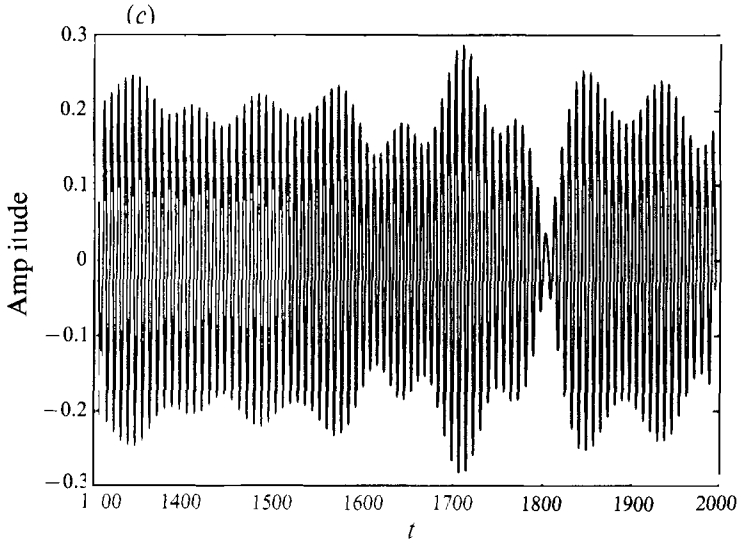

FIGURE 9. Long-term behaviour of the bed profile (at a fixed position near the channel bank) as a function of the dimensionless time t. In the numerical simulations we have set $b = 6$, $C = 0.003$, $\gamma = 1$, $r = R_c = 26.91$ and $\epsilon = 0.2$. (*a*) $q = 0.28$, which is larger than the critical value $q_c = 0.2556$. The solution of the spectral model is a Stokes wave, resulting in a regular oscillatory bed profile. (*b*) $q = 0.2$, which is between q_c and $q_H = 0.1168$. The spectral model has a periodic solution where all components Z_n have finite, non-zero amplitude. As follows from (5.20), the behaviour of the bed is quasi-periodic with two fundamental frequencies. (*c*) $q = 0.1 < q_H$. Solutions of the spectral model are quasi-periodic with two fundamental frequencies, resulting in quasi-periodic bed evolution with three fundamental frequencies.

Here, use has been made of definition (4.7), transformation (5.13) and representation (5.17).

Experiments with $q > q_c = l_c$ (see (5.16)) demonstrated that in these cases, solutions of the spectral model converge to a stable Stokes wave, for which

$$Z_0(t) = \exp(-i\alpha_2 \epsilon^2 r \tau_r t)$$

and $\hat{Z}_n(t) = 0$ for $n \neq 0$. According to (5.20), this describes a periodic alternate bar pattern. The corresponding bed profile, at a fixed position of the bank of the channel, as a function of the dimensionless time t is shown in figure 9(*a*). At $q = q_c$, the Stokes wave becomes unstable, due to a pitchfork bifurcation. For slightly smaller q-values, two new periodic solutions with $\hat{Z}_n(t) \neq 0$ for all n are observed. From (5.20) it follows that, in this case, the bed profile is composed of a series of travelling waves, each with their own wavenumber and frequency. It appears that all frequencies of this solution follow from integer combinations of two fundamental frequencies which are mutually irrational. Consequently, the temporal and spatial behaviour of the bar pattern is quasi-periodic, even though the solutions of the spectral model are periodic. An example of the bed evolution for such a situation at a fixed position near the bank as a function of time is shown in figure 9(*b*). If q is further decreased, the two periodic attractors become unstable due to a Hopf bifurcation at the critical value $q = q_H$. Solutions of the spectral model are then themselves quasi-periodic with two fundamental frequencies. As a consequence of (5.20), the bed profile become quasi-periodic with three independent frequencies. An example of the corresponding bed profile is shown in figure 9(*c*). As can be seen from (5.20)–(5.22), the bed pattern is not only quasi-periodic in time, but also in space. This behaviour is visualized in figure 10,

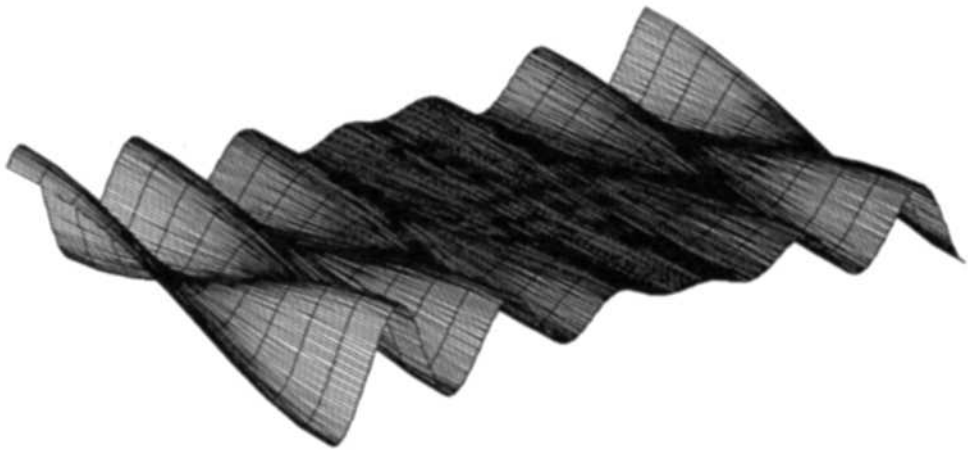

FIGURE 10. Quasi-periodic behaviour of the bed profile (at a fixed time). We have set $b = 6$, $C = 0.003$, $\gamma = 1$, $r = R_c = 26.91$, $\epsilon = 0.2$ and $q < q_H$.

which is a plot of a part of the river bed at a fixed time. The non-periodic behaviour is obvious. The role of ϵ in figure 9 can also be seen from (5.20)–(5.22): increasing ϵ causes the time- and spatial scales of the periodic and quasi-periodic behaviour to become smaller, i.e. we need shorter time and smaller distance in space to detect quasi-periodic behaviour.

So far, the preceding bifurcation scenario is similar as described by Keefe (1985) and Doelman (1991) who studied solutions of (5.19) for $\alpha_1 = 4$, $\alpha_2 = -4$. They demonstrated that for values of $q < q_H$ chaotic solutions were encountered. Within the context of morphological models, the presence of chaotic solutions would be extremely relevant, since they have limited predictability properties. However, regions with chaotic behaviour could not be located in our simulations. One reason might be that our values for q_c are an order of magnitude smaller than those found by Doelman (1991) and Keefe (1985). Since all interesting dynamical behaviour occurs in the region $0 < q < q_c$, the windows with chaotic behaviour might have become so small that they are missed by our search procedure. Alternatively, the bifurcation scenario in our case might be different, since our values for α_1 and α_2 are quite different, as can be seen from figure 7. We have not investigated these possibilities in great detail since deviations from quasi-periodic behaviour occur for small q-values. As will be demonstrated in the next section, these correspond to rather long channels which are not physically realistic.

6. Conclusions

In this paper we have studied the nonlinear behaviour of free bars generated by a unidirectional current in an infinitely long straight channel with an erodible bottom and non-erodible banks. Our main aim was to derive a modified modulation equation describing the amplitude behaviour of the bars and to demonstrate its potential importance for understanding the dynamics of free bars in rivers and laboratory tanks. We have chosen to consider a simple model which only contains the basic mechanisms responsible for bedform instabilities. Therefore, we excluded effects like the variation of the drag coefficient with the local water depth (Einstein 1950) and the dependence of the bed slope correction coefficient in the sediment transport parameterization on the bottom stress (Sekine & Parker 1992). Finally, we have assumed straight and non-

Parameter	Value	Calculated from	Determines	Value for river case	Value for tank case
k_c	0.70	(3.15)	wavelength	1975 m	39.5 m
R_c	26.97	(3.16)	channel width	220 m	4.4 m
$\lvert\omega_c\rvert$	0.77	(3.17)	wave period	9 months	9 days
$\lvert c_f\rvert$	1.11	(3.15), (3.17)	phase velocity	7 m day^{-1}	4.2 m day^{-1}
$\lvert\nu_k\rvert$	1.80	(App. B)	group velocity	11 m day^{-1}	6.8 m day^{-1}
z_b	0.86	(5.4)	bar amplitude	4.3 m	8.6 cm
q_c	0.26	(5.16)	critical q	—	—
L_c	65	(5.18)	minimum modulation length	1.43×10^4 m	286 m

TABLE 1. Model results for the parameter values $b = 6$, $C = 0.003$, $\gamma = 1$, $r = R_c$, $\epsilon = 0.8$. For the river case holds: $h_* = 5$ m, $u_* = 1$ m s^{-1}, $T = 3 \times 10^6$ s. For the tank case holds: $h_* = 0.01$ m, $u_* = 0.1$ m s^{-1}, $T = 10^5$ s.

erodible channel banks. Nevertheless, our model reproduces most of the principal aspects of the bar behaviour whereas the amount of mathematical computations is minimized, and we have demonstrated that the agreement with other linear and nonlinear studies is quite satisfactory. The model allows for a basic state, representing a uniform flow over a flat bottom, which, for sufficiently large width-to-depth ratios of the channel turned out to be unstable. A perturbation analysis of the basic state showed in linear theory that alternate bars started to develop with a certain critical wavenumber k_c and a certain critical frequency $|\omega_c|$. A weakly nonlinear theory, which is valid near critical conditions, has been applied in order to derive an amplitude equation for the marginally unstable bedforms. The procedure is similar to that presented by Colombini *et al.* (1987), who obtained a Landau equation describing the long-term behaviour of a single unstable wave. However, the situation near critical conditions is such that a narrow spectrum of waves becomes unstable. Taking that into account, we obtained a Ginzburg–Landau equation describing the evolution of the envelope amplitude of the wave group. This result also includes modulations on a long spatial scale, which are due to the dispersive properties of the wave packet. It has been demonstrated that this approach leads to situations where the periodic alternate bar pattern predicted by Colombini *et al.* (1987) can become unstable for realistic combinations of the physical parameters. It turns out that a necessary condition for instability is that the bed is dune covered.

Information on the subsequent dynamical behaviour has been obtained by cutting the channel into periodic intervals of length $2\pi/q$ and using a spectral method. It was found that q should be smaller than a critical value l_c, defined in (5.16), in order to let the Stokes solution become unstable by the sideband interaction mechanism. Physically, q_c corresponds to a minimum modulation length L_c required to observe a unstable pattern.

We have investigated if such lengths are realized in natural rivers or might be simulated in laboratory tanks. This was done by fixing the morphological parameters at $b = 6$, $C = 0.003$, $\gamma = 1$, $r = R_c$ and $\epsilon = 0.8$. In table 1 results are presented for the corresponding critical width-to-depth ratio R_c, critical wavenumber k_c, frequency $|\omega_c|$, phase velocity c_f, group velocity ν_k, characteristic amplitude $\hat{z}_b$ of the bars, the bifurcation value q_c and the corresponding minimum modulation length L_c. The results have been translated into dimensional predictions of the observed bedforms for both a typical lowland river and a laboratory tank environment. These cases have been characterized by an undisturbed water depth, the intensity of the basic uniform flow

and a morphological timescale. Of course the latter is strongly dependent on the sediment properties and has been chosen rather arbitrarily. In particular the chosen value for the laboratory tank requires very fine sediment. As noted at the end of §5, the evolution of initial perturbations of the flat bed to a fully developed bed profile takes place on a $1/\epsilon^2$ timescale. Therefore, in order to observe the periodic or quasi-periodic profiles in reality, we need lengths of laboratory tanks or natural straight reaches of the order of $1/\epsilon^2$ times the width of the tank or the river. If we then want to get realistic values, we must take ϵ of the order unity in our theory. Once the bed profile is fully developed, we may detect any quasi-periodic behaviour from the spatial structure of the profile (see figure 10).

It appears that the bar amplitudes are typically 80% of the undisturbed water depth. However, this result strongly depends on the value selected for the parameter ϵ, which measures the difference between the actual and critical width-to-depth ratio. In Colombini *et al.* (1987) order-1 values for ϵ are chosen for which the weakly nonlinear theory still yields useful results, see the discussion in §4. In this case the bar amplitudes become of the order of the undisturbed water depth which agrees better with observed alternate bars in rivers and laboratory experiments. In order for the rigid-lid approximation to be valid, the Froude number should be smaller than approximately 0.1, as can be traced back from (2.9)–(2.12). This poses rather strong conditions on the intensity of the basic flow which, especially in the case of laboratory tank experiments, are difficult to meet. Furthermore, it is found that the minimum modulation length is approximately 65 channel width units. Both for the river and the tank situation this condition might possibly be satisfied. Our experiments have shown that in these cases the bed profiles behave quasi-periodically, both in space and in time. Although the evolution seems rather complicated, see the time series in figure 9, the dynamics are still perfectly predictable. In principle the Ginzburg–Landau equation also allows for chaotic solutions with associated limited predictability properties (Keefe 1985; Doelman 1991). However, they were not observed in our simulations, resulting in the conclusion that they might only occur for an extremely small region of q-values. Thus the occurrence of chaos seems not very relevant within the context of the present model.

We thank H. J. de Vriend, E. Mosselman, and the referees for useful suggestions and comments.

Appendix A

The asymptotic results for α_u, α_v and α_ζ, defined in (3.8), read as follows:

$$\alpha_u = \delta^{\frac{1}{2}}\{1-5\delta^{\frac{1}{2}}+O(\delta)\}+\mathrm{i}\tfrac{1}{2}\sqrt{2}\delta^{\frac{1}{4}}\{1+O(\delta)\},$$
$$\alpha_v = \delta^{\frac{1}{2}}\{1+O(\delta)\}+\mathrm{i}\tfrac{1}{2}\sqrt{2}\delta^{\frac{1}{4}}\{1-\delta^{\frac{1}{2}}+O(\delta)\},$$
$$\alpha_\zeta = -2\delta^{\frac{1}{2}}\{1-\tfrac{3}{2}\delta^{\frac{1}{2}}+O(\delta)\}+\mathrm{i}2\sqrt{2}\delta^{\frac{3}{4}}\{1+\tfrac{1}{2}\delta^{\frac{1}{2}}+O(\delta)\}.$$

Below, we show the asymptotic results for the solutions of the equations $\boldsymbol{L}_{02}\boldsymbol{\phi}_{02}=\boldsymbol{f}_{02}$ and $\boldsymbol{L}_{22}\boldsymbol{\phi}_{22}=\boldsymbol{f}_{22}$ which were considered in §4. In (4.15),

$$\boldsymbol{\phi}_{02} = |A|^2\begin{pmatrix} u_{02\mathrm{s}}\sin^2(\pi y)+u_{02\mathrm{c}}\cos^2(\pi y) \\ v_{02}\sin(2\pi y) \\ \zeta_{02}\cos(2\pi y) \\ z_{02}\cos(2\pi y)\end{pmatrix},$$

where

$$u_{02s} = \frac{-4+3b}{4(b-1)} - \left(3+\frac{b(1+b)}{4(b-1)}\right)\delta^{\frac{1}{2}} + O(\delta),$$

$$u_{02c} = -\frac{(-4+3b)}{4(b-1)} + \left(-\frac{5}{2}+\frac{b(1+b)}{4(b-1)}\right)\delta^{\frac{1}{2}} + O(\delta),$$

$$v_{02} = \delta^{\frac{1}{2}} + O(\delta^{\frac{6}{4}}), \quad z_{02} = \frac{-b}{2(b-1)} - \frac{b(1+b)\,\delta^{\frac{1}{2}}}{2(b-1)} + O(\delta);$$

and in (4.17),

$$\boldsymbol{\phi}_{22} = A^2 \begin{pmatrix} u_{22s}\sin^2(\pi y) + u_{22c}\cos^2(\pi y) \\ v_{22}\sin^2(\pi y) \\ \zeta_{22s}\sin^2(\pi y) + \zeta_{22c}\cos^2(\pi y) \\ z_{22s}\sin^2(\pi y) + z_{22c}\cos^2(\pi y) \end{pmatrix},$$

where

$$u_{22s} = \frac{-1}{6(b-1)} - \frac{\sqrt{2}\,\mathrm{i}(b-6)}{12(b-1)}\delta^{\frac{1}{4}} + \frac{(21-24b+b^2)}{12(b-1)}\delta^{\frac{1}{2}} + \frac{\sqrt{2}\,\mathrm{i}(-47+29b-b^2)}{12(b-1)}\delta^{\frac{3}{4}} + O(\delta),$$

$$u_{22c} = \frac{1}{6(b-1)} + \frac{\sqrt{2}\,\mathrm{i}(-12+b)}{12(b-1)}\delta^{\frac{1}{4}} + \frac{(-45+33b+2b^2)}{12(b-1)}\delta^{\frac{1}{2}} + \frac{\sqrt{2}\,\mathrm{i}(59-41-5b^2)}{12(b-1)}\delta^{\frac{3}{4}} + O(\delta),$$

$$v_{22} = \frac{2}{3(b-1)} + \frac{\sqrt{2}\,\mathrm{i}(-8+5b)}{6(b-1)}\delta^{\frac{1}{4}} + \frac{(-29+20b+b^2)}{6(b-1)}\delta^{\frac{1}{2}} + \frac{\sqrt{2}\,\mathrm{i}(-116-3b)}{24(b-1)}\delta^{\frac{3}{4}} + O(\delta),$$

$$z_{22s} = \frac{\sqrt{2}\,\mathrm{i}}{3(b-1)}\delta^{-\frac{1}{4}} - \frac{b-2}{3(b-1)} + \frac{\sqrt{2}\,\mathrm{i}(-20+16b+b^2)}{12(b-1)}\delta^{\frac{1}{4}} + \frac{-62+53b+5b^2}{24(b-1)}\delta^{\frac{1}{2}} + O(\delta^{\frac{3}{4}}),$$

$$z_{22c} = \frac{-\mathrm{i}\sqrt{2}}{3(b-1)}\delta^{-\frac{1}{4}} + \frac{b-2}{3(b-1)} + \frac{\mathrm{i}\sqrt{2}(20-22b-b^2)}{12(b-1)}\delta^{\frac{1}{4}} + \frac{38-59b+b^2}{24(b-1)}\delta^{\frac{1}{2}} + O(\delta^{\frac{3}{4}}).$$

Note that the expressions for ζ_{02c} and ζ_{22s} are omitted. It appeared that they were not necessary for the derivation of the nonlinear term of the Ginzburg–Landau equation. This is due to the assumption that the Froude number is small, which physically means that there are no dynamical effects due to variations in the water surface.

Appendix B

In this Appendix we shall specify the expressions that appear in the inhomogeneous term $\tilde{g}$, (4.29), as used in the weakly nonlinear analysis. For convenience we write k and R where we mean k_c and R_c. First, we define the following quantities:

$$f^u_{13} = f^u_{13,1} + f^u_{13,2}\cos(\pi y) + |A|^2 A[f^u_{13,3}\sin^2(\pi y)\cos(\pi y) + f^u_{13,4}\cos^3(\pi y)],$$

$$f^v_{13} = f^v_{13,1} + f^v_{13,2}\sin(\pi y) + |A|^2 A[f^v_{13,3}\cos^2(\pi y)\sin(\pi y) + f^v_{13,4}\sin^3(\pi y)],$$

$$f^\zeta_{13} = f^\zeta_{13,1} + f^\zeta_{13,2}\cos(\pi y) + |A|^2 A[f^\zeta_{13,3}\sin^2(\pi y)\cos(\pi y) + f^\zeta_{13,4}\cos^3(\pi y)],$$

$$f^z_{13} = f^z_{13,1} + f^z_{13,2}\cos(\pi y) + |A|^2 A[f^z_{13,3}\sin^2(\pi y)\cos(\pi y) + f^z_{13,4}\cos^3(\pi y)],$$

where the first two terms in the right-hand sides are linear in ϕ_{11} and ϕ_{12} (they follow from the theory developed in §4 and are thus not of concern here) and where

$$
\begin{aligned}
f^u_{13,3} &= -(\tfrac{1}{2}\alpha_v^2+\alpha_v\overline{\alpha_v})\,CR-\mathrm{i}k(\alpha_u u_{02\mathrm{s}}+\overline{\alpha_u}u_{22\mathrm{s}})\\
&\quad -2\pi[\alpha_v(-u_{02\mathrm{c}}+u_{02\mathrm{s}})+\overline{\alpha_v}(-u_{22\mathrm{c}}+u_{22\mathrm{s}})]+2\pi(\alpha_u v_{02}+\overline{\alpha_u}v_{22})\\
&\quad -2CR[\alpha_v v_{02}+\overline{\alpha_v}v_{22}+(1+\alpha_u)(u_{02\mathrm{s}}-z_{02})+(1+\overline{\alpha_u})(u_{22\mathrm{s}}+z_{22\mathrm{s}})],\\
f^u_{13,4} &= -(1+\alpha_u)(1+\alpha_u+2(1+\overline{\alpha_u}))\,CR-\mathrm{i}k(\alpha_u u_{02\mathrm{c}}+\overline{\alpha_u}u_{22\mathrm{c}})\\
&\quad -2CR[(1+\alpha_u)(u_{02\mathrm{c}}+z_{02})+(1+\overline{\alpha_u})(u_{22\mathrm{c}}+z_{22\mathrm{c}})],\\
f^v_{13,3} &= -\mathrm{i}k(\alpha_v u_{02\mathrm{c}}-\overline{\alpha_v}u_{22\mathrm{c}}+4\overline{\alpha_u}v_{22})\\
&\quad -2CR[(1+\alpha_u)v_{02}+(1+\overline{\alpha_u})v_{22}]-4\pi(\alpha_v v_{02}+\overline{\alpha_v}v_{22})\\
&\quad -\alpha_v CR(2+\alpha_u+\overline{\alpha_u}+u_{02\mathrm{c}}+z_{02})-\overline{\alpha_v}CR(1+\alpha_u+u_{22\mathrm{c}}+z_{22\mathrm{c}}),\\
f^v_{13,4} &= -\mathrm{i}k(\alpha_v u_{02\mathrm{s}}-\overline{\alpha_v}u_{22\mathrm{s}})+2\pi(\alpha_v v_{02}+\overline{\alpha_v}v_{22})\\
&\quad -CR[1\tfrac{1}{2}\alpha_v^2\overline{\alpha_v}+\alpha_v(u_{02\mathrm{s}}-z_{02})+\overline{\alpha_v}(u_{22\mathrm{s}}+z_{22\mathrm{s}})],\\
f^\zeta_{13,3} &= -4\pi(v_{02}+v_{22})-5\pi\alpha_v z_{02}+\pi\overline{\alpha_v}(-2z_{22\mathrm{c}}+3z_{22\mathrm{s}})+\mathrm{i}k(u_{02\mathrm{s}}+u_{22\mathrm{s}}-\alpha_u z_{02}+\overline{\alpha_u}z_{22\mathrm{s}}),\\
f^\zeta_{13,4} &= \mathrm{i}k(u_{02\mathrm{c}}+u_{22\mathrm{c}}+\alpha_u z_{02}+\overline{\alpha_u}z_{22\mathrm{c}})+\pi(2(v_{02}+v_{22})+\alpha_v z_{02}+\overline{\alpha_v}z_{\mathrm{s}22\mathrm{c}}),\\
f^z_{13,3} &= \pi(b-1)[-\tfrac{9}{2}\alpha_v^2\overline{\alpha_v}+(b-2)(2\alpha_u\overline{\alpha_u}\alpha_v+\alpha_u^2\overline{\alpha_v})]\\
&\quad +\pi(b-1)[\alpha_v(2u_{02\mathrm{c}}-3u_{02\mathrm{s}})+\overline{\alpha_v}(2u_{22\mathrm{c}}-3u_{22\mathrm{s}})+4(\alpha_u v_{02}+\overline{\alpha_u}v_{22})]\\
&\quad -(b-1)\,\mathrm{i}k[\tfrac{1}{2}(b-2)(\overline{\alpha_u}\alpha_v^2+2\alpha_u\alpha_v\overline{\alpha_v})+b(\alpha_u u_{02\mathrm{s}}+\overline{\alpha_u}u_{22\mathrm{s}})+2(\alpha_v v_{02}+\overline{\alpha_v}v_{22})]\\
&\quad -(\gamma/R)\,bk^2(-\tfrac{1}{2}\alpha_u+\alpha_v\overline{\alpha_v}+u_{02\mathrm{s}}-u_{22\mathrm{s}}+2\overline{\alpha_u}z_{22\mathrm{s}})\\
&\quad -3\pi^2 b(\gamma/R)(\tfrac{1}{2}\alpha_v^2+\alpha_v\overline{\alpha_v}+u_{02\mathrm{s}}+u_{22\mathrm{s}})\\
&\quad +2\pi^2 b(\gamma/R)[\tfrac{1}{2}\alpha_u^2(b-1)+\alpha_u\overline{\alpha_u}(b-1)+u_{02\mathrm{c}}+u_{22\mathrm{c}}+4\alpha_u z_{02}-2\overline{\alpha_u}(-z_{22\mathrm{c}}+z_{22\mathrm{s}})],\\
f^z_{13,4} &= -\tfrac{1}{2}\pi(b-1)(b-2)(2\alpha_u\overline{\alpha_u}\alpha_v+\alpha_u^2\overline{\alpha_v})\\
&\quad -b(b-1)\,\mathrm{i}k(\tfrac{1}{2}\alpha_u^2\overline{\alpha_u}(b-2)+\alpha_u u_{02\mathrm{c}}+\overline{\alpha_u}u_{22\mathrm{c}})\\
&\quad -\pi(b-1)[\alpha_v u_{02\mathrm{c}}+\overline{\alpha_v}u_{22\mathrm{c}}+2(\alpha_u v_{02}+\overline{\alpha_u}v_{22})]\\
&\quad -(\gamma/R)\,bk^2[-\tfrac{1}{2}\alpha_u^2(b-1)+\alpha_u\overline{\alpha_u}(b-1)+u_{02\mathrm{c}}-u_{22\mathrm{c}}+2\overline{\alpha_u}z_{22\mathrm{c}}]\\
&\quad -\pi^2 b(\gamma/R)[\tfrac{1}{2}\alpha_u^2(b-1)+\alpha_u\overline{\alpha_u}(b-1)+u_{02\mathrm{c}}+u_{22\mathrm{c}}+4\alpha_u z_{02}-2\overline{\alpha_u}(-z_{22\mathrm{c}}+z_{22\mathrm{s}})].
\end{aligned}
$$

We shall now specify g_i, $i=1,\ldots,4$, as they appear in (4.29):

$$
\begin{aligned}
g_1 &= -k^2(\mathrm{i}k+CR)[f^z_{13,1}-bf^\zeta_{13,1}],\\
g_2 &= -k^2(\mathrm{i}k+CR)[f^z_{13,2}-bf^\zeta_{13,2}]-\pi^2((\mathrm{i}k+2CR)[f^z_{13,2}-bf^\zeta_{13,2}]\\
&\quad +\pi^2\mathrm{i}k(b-1)f^u_{13,2}-\pi(b-1)k^2 f^v_{13,2},\\
g_3 &= -7\pi^2(-f^s_{13,3}+f^z_{13,3})(2CR+\mathrm{i}k)+6\pi^2(-f^\zeta_{13,4}+f^z_{13,4})(2CR+\mathrm{i}k)\\
&\quad +7\mathrm{i}\pi^2k(b-1)f^u_{13,3}-6\mathrm{i}\pi^2k(b-1)f^u_{13,4}+2\pi(b-1)f^v_{13,3}k^2-3\pi(b-1)f^v_{13,4}k^2\\
&\quad -(CR+\mathrm{i}k)k^2(f^z_{13,3}-bf^\zeta_{13,3}),\\
g_4 &= 2\pi^2(-f^\zeta_{13,3}+f^z_{13,3})(2CR+\mathrm{i}k)-3\pi^2(-f^\zeta_{13,4}+f^z_{13,4})(2CR+\mathrm{i}k)\\
&\quad -2\mathrm{i}\pi^2(b-1)f^u_{13,3}k+3\mathrm{i}\pi^2(b-1)f^u_{13,4}k-\pi(b-1)f^v_{13,3}k^2\\
&\quad -(CR+\mathrm{i}k)k^2(f^z_{13,4}-bf^\zeta_{13,4}).
\end{aligned}
$$

Working out the solvability condition (4.30) (thereby using the terms in f_{13} that are linear in ϕ_{11} and ϕ_{12}) results in the Ginzburg–Landau equation:

$$\frac{\partial A}{\partial \tau} = r\frac{\partial \omega}{\partial R}A - \frac{1}{2}\frac{\partial^2 \omega}{\partial k^2}\frac{\partial^2 A}{\partial \xi^2} - \frac{1}{4}\left[\frac{g_3+3g_4}{k^2(\mathrm{i}k+CR)+\pi^2(\mathrm{i}k+2CR)}\right]|A|^2 A$$

$$= r(\tau_r+\mathrm{i}\nu_r)A - \tfrac{1}{2}(\tau_{k^2}+\mathrm{i}\nu_{k^2})\frac{\partial^2 A}{\partial \xi^2} + (c_r+\mathrm{i}c_i)|A|^2 A,$$

where

$$\tau_r = \frac{2\delta\beta^2}{\gamma}(1-4\delta^{\frac{1}{2}}+O(\delta)), \quad \nu_r = \frac{2\sqrt{2}\,\beta^2\delta^{\frac{5}{4}}}{\gamma}(1-3\delta^{\frac{1}{2}}+O(\delta)),$$

$$\tau_{k^2} = \frac{-8\beta\delta^{\frac{1}{2}}}{\pi}(1+2\delta^{\frac{1}{2}}+O(\delta)), \quad \nu_{k^2} = \frac{-5\sqrt{2}\,\beta\delta^{\frac{1}{4}}}{\pi}(1-6\delta^{\frac{1}{2}}+O(\delta)),$$

$$c_i = \frac{(20-30b+9b^2)\sqrt{2}\,\pi}{24(b-1)}\delta^{\frac{1}{4}} + \frac{(-162+294b-133b^2+15b^3)\sqrt{2}\,\pi}{24(b-1)}\delta^{\frac{3}{4}} + O(\delta^{\frac{5}{4}}),$$

$$c_r = -\frac{2\pi}{3(b-1)} + \frac{(62-78b+19b^2-9b^3)\pi}{12(b-1)}\delta^{\frac{1}{2}} + O(\delta).$$

The expression for the group velocity reads

$$\nu_k = -\{1+7(b-1)\,\delta^{\frac{1}{2}} - 18(b-1)\,\delta + O(\delta^{\frac{3}{2}})\}.$$

REFERENCES

BAGNOLD, R. A. 1956 The flow of cohesionless grains in fluids. *Proc. R. Soc. Lond.* A **249**, 235–279.

BENJAMIN T. B. & FEIR, J. E. 1967 The disintegration of wave trains on deep water. Part 1. Theory. *J. Fluid Mech.* **27**, 417–430.

BLENNERHASSET, P. J. 1980 On the generation of waves by wind. *Phil. Trans. R. Soc. Lond.* **298**, 451–494.

BLONDEAUX, P. & SEMINARA, G. 1985 A unified bar bend theory of river meanders. *J. Fluid Mech.* **157**, 449–470.

CALLANDER, R. A. 1969 Instability and river channels. *J. Fluid Mech.* **36**, 465–480.

COLOMBINI, M., SEMINARA, G. & TUBINO, M. 1987 Finite-amplitude alternate bars. *J. Fluid Mech.* **181**, 213–232.

CROSATO, A. 1989 Simulation of meandering river processes. *Commun. Hydraul., Rep.* 3-90, Delft Univ. of Technology.

DOELMAN, A. 1989 Slow time periodic solutions of the Ginzburg–Landau equation. *Physica* D **40**, 156–172.

DOELMAN, A. 1991 Finite dimensional models of the Ginzburg–Landau equation. *Nonlinearity* **4**, 231–250.

DOERING, C. R., GIBBON, J. D., HOLM, D. D. & NICOLAENCO, B. 1988 Low dimensional behaviour in the complex Ginzburg–Landau equation. *Nonlinearity* **1**, 279–309.

DRAZIN, P. G. & REID, W. H. 1981 *Hydrodynamic Stability*. Cambridge University Press.

EINSTEIN, H. A. 1950 The bedload function for sediment transport in open channel flow. *US Dept. Agric. Tech. Bull.* 1026.

ENGELUND, F. 1974 Flow and bed topography in channel bends. *J. Hydr. Div., ASCE* **100** (HY11), 1631–1648.

ENGELUND, F. & SKOVGAARD, O. 1973 On the origin of meandering and braiding in alluvial streams. *J. Fluid Mech.* **57**, 289–302.

FREDSØE, J. 1978 Meandering and braiding of rivers. *J. Fluid Mech.* **84**, 609–624.

FUKUOKA, S. 1989 Finite amplitude development of alternate bars. In *River Meandering* (ed. Ikeda, S. & Parker, G.). AGU *Water Resources Monograph*, vol. 12, pp. 237–266. Washington DC.

KEEFE, L. R. 1985 Dynamics of perturbed wavetrain solutions to the Ginzburg–Landau equation. *Stud. Appl. Maths* **73**, 91–153.

KURAMOTO, Y. 1984 Chemical Oscillations, Waves and Turbulence. Springer.

LIGHTHILL, J. 1978 *Waves in Fluids*. Cambridge University Press.

MATKOWSKI, B. J. & VOLPERT, V. 1993 Stability of plane wave solutions of complex Ginzburg–Landau equation. *Q. Appl. Maths* (to appear).

NEWELL, A. C. 1974 Envelope equations. *Lect. Appl. Maths* **15**, 157–163.

NEWELL, A. C. & WHITEHEAD, J. A. 1969 Finite bandwidth, finite amplitude convection. *J. Fluid Mech.* **28**, 279–303.

OLESEN, K. 1983 Alternate bars in and meandering of alluvial rivers. *Commun. Hydraul., Rep.* 7-83. Delft Univ. of Technology.

PARKER, G. 1976 On the cause and characteristic scales of meandering and braiding in rivers. *J. Fluid Mech.* **76**, 457–480.

PARKER, G. & JOHANNESSON, H. 1989 Observations of several recent theories of resonance and overdeepening in meandering channels. I *River Meandering* (ed. Ikeda, S. & Parker, G.). AGU *Water Resources Monograph*, vol. 12, pp. 379–415. Washington DC.

RIJN, L. C. VAN 1989 *Handbook of Sediment Transport by Currents and Waves*. Delft Hydraulics, Delft, The Netherlands.

ROZOVSKIJ, I. L. 1957 *Flow of Water in Bends of Open Channels*. Kiev: Acad. Sci. Ukranian SSR.

SCHÖPF, W. & ZIMMERMANN, W. 1989 Multicritical behaviour in binary fluid convection. *Europhys. Lett.* **8**, 41–46.

SEKINE, M. & PARKER, G. 1992 Bed-load transport on transverse slope. *J. Hydraul. Engng ASCE* **118** (4), 513–535.

STEWARTSON, K. & STUART, J. T. 1971 A nonlinear instability theory for a wave system in plane Poiseuille flow. *J. Fluid Mech.* **48**, 529–545.

STUART, J. T. & DIPRIMA, R. C. 1978 The Eckhaus and Benjamin–Feir resonance mechanisms. *Proc. R. Soc. Lond.* A **362**, 27–41.